



# LUND UNIVERSITY

## On Automation of the PID Tuning Procedure

Soltesz, Kristian

2012

*Document Version:*

Publisher's PDF, also known as Version of record

[Link to publication](#)

*Citation for published version (APA):*

Soltesz, K. (2012). *On Automation of the PID Tuning Procedure*. [Licentiate Thesis, Department of Automatic Control]. Department of Automatic Control, Lund Institute of Technology, Lund University.

*Total number of authors:*

1

### General rights

Unless other specific re-use rights are stated the following general rights apply:

Copyright and moral rights for the publications made accessible in the public portal are retained by the authors and/or other copyright owners and it is a condition of accessing publications that users recognise and abide by the legal requirements associated with these rights.

- Users may download and print one copy of any publication from the public portal for the purpose of private study or research.
- You may not further distribute the material or use it for any profit-making activity or commercial gain
- You may freely distribute the URL identifying the publication in the public portal

Read more about Creative commons licenses: <https://creativecommons.org/licenses/>

### Take down policy

If you believe that this document breaches copyright please contact us providing details, and we will remove access to the work immediately and investigate your claim.

LUND UNIVERSITY

PO Box 117  
221 00 Lund  
+46 46-222 00 00



# LUND UNIVERSITY

## On Automation of the PID Tuning Procedure

Soltesz, Kristian

Published: 2012-01-01

[Link to publication](#)

*Citation for published version (APA):*

Soltesz, K. (2012). On Automation of the PID Tuning Procedure Department of Automatic Control, Lund Institute of Technology, Lund University

### General rights

Copyright and moral rights for the publications made accessible in the public portal are retained by the authors and/or other copyright owners and it is a condition of accessing publications that users recognise and abide by the legal requirements associated with these rights.

- Users may download and print one copy of any publication from the public portal for the purpose of private study or research.
- You may not further distribute the material or use it for any profit-making activity or commercial gain
- You may freely distribute the URL identifying the publication in the public portal ?

### Take down policy

If you believe that this document breaches copyright please contact us providing details, and we will remove access to the work immediately and investigate your claim.

LUND UNIVERSITY

PO Box 117  
221 00 Lund  
+46 46-222 00 00

# On Automation of the PID Tuning Procedure

Kristian Soltesz

Department of Automatic Control  
Lund University  
Lund, January 2012

Department of Automatic Control  
Lund University  
Box 118  
SE-221 00 LUND  
Sweden

ISSN 0280-5316  
ISRN LUTFD2/TFRT--3254--SE

© 2012 by Kristian Soltesz. All rights reserved.  
Printed in Sweden,  
Lund University, Lund 2012

# Abstract

Within process industry, and in many other areas, the PID controller is responsible for handling regulatory control. An educated guess is that the number of executing PID control loops lies in the billions (2011) and there are no signs indicating a decrease of this number.

Properly tuning the PID controller, i.e., setting its parameter values based on characteristics of the process it controls together with robustness criteria, is commonly both timely and costly. Hence, the tuning is often overseen, resulting in numerous poorly tuned loops. These result in unnecessary lack of performance, which might be both hazardous and uneconomic.

If a linear time invariant model of the process is given, there exists numerous feasible tuning methods. However, automatically obtaining even a low complexity model is far from trivial in the absence of a priori process information.

This thesis addresses system identification to be used in the automatic PID tuning procedure. A method for generating the identification input signal is proposed. Its objective is to yield higher model accuracy in the frequency range where it is most needed for robust tuning.

Subsequently, methods for obtaining process models from input and output data pairs are proposed and discussed. All methods are presented using numerous simulations and laboratory experiments.

Finally, a simulation study of closed-loop anesthesia in human patients, based on clinically obtained model parameters, is presented. The novelty lies in that the depth of hypnosis PID controller is individualized based on data collected during the induction phase of anesthesia. It is demonstrated that updating the controller, using a herein proposed method, significantly improves performance.



# Acknowledgments

It is with the direct or indirect help from several persons that I have come to write this thesis. With the reservation of forgetting anyone of you, I would explicitly like to acknowledge the following persons.

My supervisor Professor Tore Hägglund has been ever supporting in my work. Your engagement and mentoring has meant a lot to me. You have always encouraged me and contributed to an atmosphere in which it has been truly enjoyable to work. You have also served as a role model, in a much broader context than that of automatic control.

Professor Karl Johan Åström has been a great source of inspiration and has been the source of several key ideas around which I have worked.

The administrative staff at the department, being Britt-Marie Mårtensson, Ingrid Nilsson, Eva Schildt, Agneta Tuszynski and Eva Westin have all been very kind, knowledgeable and helpful.

At the University of British Columbia I would like to acknowledge Professor Guy Dumont and Post Doctoral Fellow Jin-Oh Hahn for introducing me to an interesting research topic.

Thank you office mates Magnus Linderöth, Anna Lindholm and Alina Rubanova as well as adjacent office mates Karl Berntorp and Philip Reuterswärd for interesting discussions; both work related in the office and more general in the coffee room. Especially, thank you Magnus for all time and effort spent discussing interesting problems.

Research Engineers Rolf Braun, Anders Blomdell and Leif Andersson have taught me many interesting things related to computers, lab processes and workshop machines which I am sure will come to use regularly.

Finally I would like to thank Ingrid, my family and friends.



# Contents

<b>1. Introduction</b> . . . . .	9
1.1 Background . . . . .	9
1.2 Motivation . . . . .	14
<b>2. Synopsis</b> . . . . .	21
2.1 Contributions . . . . .	21
<b>References</b> . . . . .	24
<b>Paper I. Extending the Relay Feedback Experiment</b> . .	<b>27</b>
1. Introduction . . . . .	28
2. Problem formulation and Approach . . . . .	32
3. Simulation Results . . . . .	40
4. Physical Example . . . . .	40
5. Conclusion . . . . .	43
6. Future Work . . . . .	44
References . . . . .	46
<b>Paper II. Transfer Function Parameter Identification by Modified Relay Feedback</b> . . . . .	<b>47</b>
1. Introduction . . . . .	48
2. Optimization Method for Identification . . . . .	49
3. FOTD Model Identification . . . . .	52
4. Experimental Procedure . . . . .	57
5. Results . . . . .	58
6. Conclusions . . . . .	62
7. Future Work . . . . .	63
References . . . . .	64

<b>Paper III. Individualized PID Control of Depth of Anesthesia Based on Patient Model Identification During the Induction Phase of Anesthesia . . . . .</b>	<b>65</b>
1. Introduction . . . . .	66
2. Model of the Propofol-DOH Process . . . . .	67
3. Robust PID Control Synthesis . . . . .	73
4. System Identification . . . . .	77
5. Simulated Experiment . . . . .	80
6. Results and Discussion . . . . .	81
7. Conclusion . . . . .	83
References . . . . .	84

# 1

## Introduction

### 1.1 Background

#### An Overview

The main topic of this thesis is the automation of the PID tuning procedure. In its simplest form, this comes down to determining the parameter set  $\{K, T_i, T_d\}$  of the PID control law

$$u(t) = K \left( e(t) + \frac{1}{T_i} \int_0^t e(\tau) d\tau + T_d \frac{d}{dt} e(t) \right), \quad (1.1)$$

relating the control signal  $u$  to the current and past control error  $e$ . Due to practical considerations regarding for example periodic execution, measurement noise and actuator limits, the control law (1.1) is subject to modifications prior to implementation in a digital computer. These modifications are discussed extensively in e.g. [Åström and Wittenmark, 1996]. In practice, the choice of controller parameters is often based on human insight and prior experience. A more systematic approach to controller tuning bases the parameter choice on:

1. A model of the process to be controlled.
2. Performance specifications on the controlled system.

A process model is any set of characteristics describing the process. Here we will only consider single input single output (SISO) processes.

In the context of (PID) controller tuning it is common and convenient to approximate the process dynamics with a linear time invariant (LTI) model, possibly with a time delay between the input and output. Most processes suited for PID control can be adequately modeled by a low order, well-damped, LTI system around the reference operating point. Focus will therefore lie on first order time delayed (FOTD):

$$G_1(s) = \frac{K}{sT + 1} e^{-sL} \quad (1.2)$$

and second order time delayed (SOTD):

$$G_2(s) = \frac{b_1s + b_2}{s^2 + a_1s + a_2} e^{-sL} \quad (1.3)$$

systems.

Performance specifications may vary depending on application and generally constitute a trade-off between conflicting interests such as fast disturbance attenuation and robustness towards model uncertainties. Once a model is obtained, there exist numerous methods to determine the controller parameters. The most famous of these are arguably those due to Ziegler and Nichols [Ziegler and Nichols, 1942]. Over the years, numerous additional tuning regimens, such as [Hägglund and Åström, 2002], [Garpinger and Hägglund, 2008] and [Skogestad, 2003] have been introduced.

This work focuses on obtaining a process model, rather than how to use one to determine a controller tuning to match the performance specifications. The purpose is to identify parameters of a model with the structure of (1.2) or (1.3), based on an input signal  $u(t)$  and the corresponding system output  $y(t)$ . Such an identification procedure normally consists of separate experiment design and parameter identification stages. During the experiment design stage, the input  $u(t)$  is synthesized. It is important that  $u$  excites the dynamics of the process and hence establishes an appropriate signal to noise ratio in the frequency range of interest. Typically this frequency range lies around the bandwidth of the open loop system. Once an input has been determined and applied to the system and the corresponding output  $y$  has been recorded, the pair  $\{u, y\}$  is used to determine the parameters of the process model.

The traditional approach to system identification often involves iterating over the experiment design and parameter identification stages. This generally involves human interaction and a skilled engineer can contribute significantly towards efficiently obtaining a good model.

In the context of automated PID tuning, it is desired to automate both the identification and tuning procedure, enabling a cheap and time-wise efficient execution, which can be directly applied at the site where the control loop is located. This puts new demands on the identification procedure:

- The procedure should work on processes with varying time scales and dynamics.
- Little, or no, a priori information is known at the start of the automatic procedure.
- Experiment duration need to be kept short.

Most processes in the regulatory control layer [Skogestad, 2004] of a process industrial plant, which is where the PID controllers are found, are stable and a majority exhibit monotonous step responses. Set-point changes are generally rare and the main role of the PID controller is therefore that of disturbance rejection around a given set-point.

In this process industrial setting it is realistic to assume that the process to be identified is stable, has a monotonous step response and can be adequately modeled within the structure of (1.2) or (1.3). In addition to this, the proposed method will handle integrating processes, which are found in several process industrial applications.

### The Relay Auto-Tuning Experiment

The perhaps most well-known automatic PID tuning procedure is the relay feedback experiment [Åström and Hägglund, 1984]. The aim of the experiment is to tune a PID controller  $C$  to regulate the unknown dynamics of a process  $P$ . A schematic sketch of the relay auto-tuner is shown in Fig. 1.1. It is assumed that  $y = 0$  corresponds to a dynamical equilibrium, constituting the operating point of the system. (For an operating point corresponding to  $y \neq 0$ , an affine scaling of  $u$  and  $y$  must first be performed.)

In tuning mode, the feedback path is closed over the relay, rather than  $C$ . For a large family of processes, this causes a stable oscillation.

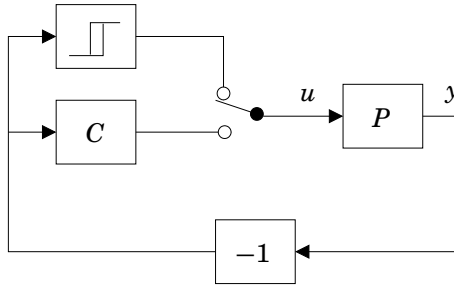


**Figure 1.1** Schematic sketch of the relay auto-tuner.

The stable FOTD case is completely described in [Lin *et al.*, 2004]. Experience has shown that stable, well-damped, monotonous step response processes generally result in well-behaved oscillations under relay feedback. However, there also exist cases where the relay oscillations exhibit esoteric properties [Johansson *et al.*, 2002].

The relay output amplitude  $d$  needs to be chosen such that the closed-loop oscillations have a high enough amplitude to be distinguishable from noise in  $y$ , while not deviating unnecessarily far from the operating point of  $P$ .

An approximation of the oscillation frequency and amplitude are available through describing function analysis. The describing function of the relay nonlinearity is given by

$$N(a) = \frac{4d}{a\pi}, \quad (1.4)$$

where  $a$  is the input amplitude. Hence, its negative reciprocal intersects the Nyquist curve of  $C$  along the negative real axis.

In order to tolerate noise in  $y$ , a symmetric hysteresis  $\pm h$  is normally introduced in the relay. This changes the describing function into fulfilling

$$-\frac{1}{N(a)} = -\frac{\pi a}{4d} \left( \sqrt{1 - \left(\frac{h}{a}\right)^2} + i\frac{h}{a} \right). \quad (1.5)$$

It is hence a vertically shifted (and scaled) version of (1.4), as shown in Fig. 1.2.

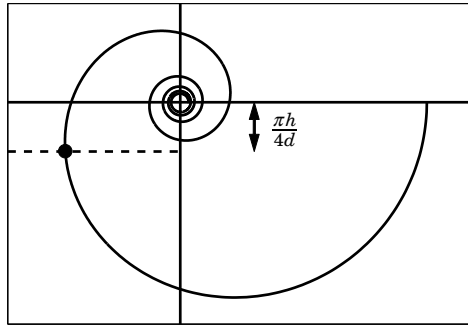


**Figure 1.2** Point on the process Nyquist curve obtained by relay feedback experiment with relay hysteresis  $h$ .

In the traditional relay tuner, a direct method is used. The angular frequency  $\omega_{180}$  of the oscillation base harmonic and the corresponding amplitude  $a$  are used to determine the parameters of  $C$  through

$$[K, T_i, T_d] = f(\omega_{180}, a), \quad (1.6)$$

for some function  $f$ . This is opposed to indirect methods, where  $\omega_{180}$  and  $a$  would first be used to identify parameters of a process model  $\hat{P}$ , which, in terms, are used to determine  $\{K, T_i, T_d\}$ .

The relay auto-tuner has successfully been implemented in several commercially available devices, e.g. from ABB and Fisher Controls (bought by Emerson).

Since the relay feedback experiment only identifies one point on the process Nyquist curve, there is an inherent ambiguity associated with the method. For example, the two Nyquist curves in Fig. 1.3 represent significantly different dynamics and it is likely that one would choose different tunings of  $C$  for each of them. However, they both correspond to processes with the same critical gain, and so the relay feedback experiment would result in the same tuning for both dynamics. Because of this, extensions have been made to the classic relay auto-tuner. For instance, repeated experiments with varied relay hys-

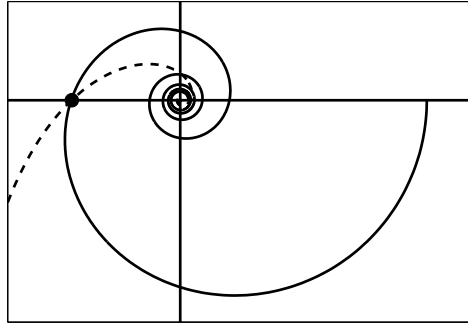


**Figure 1.3** Nyquist curves of two process models with differing dynamics, but the same critical gain.

teresis can be used to identify several points on the Nyquist curve of  $P$ . A natural problem in this setting is which hysteresis values should be used. Fig. 1.4 demonstrates this problem; the three hysteresis values chosen make sense in one of the cases (solid Nyquist curve), but not for the other (dashed Nyquist curve).

In [Friman and Waller, 1997], the relay is exchanged for a nonlinearity which allows identification of a point corresponding to a predetermined third quadrant phase angle of  $P$ . This is more appealing than changing the relay hysteresis, since it identifies significant points on the Nyquist curve regardless of  $P$ , as illustrated by Fig. 1.5. However, it still requires repeated experiments, during all of which a stable oscillation need to be reached.

## 1.2 Motivation

### PID in Process Industry

PID control is an old and widely used technology. The PI controller dates back to the era of steam engines. It has survived two paradigm

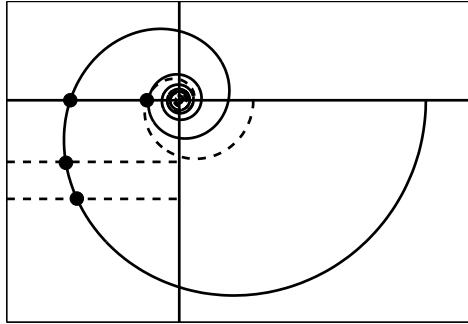


**Figure 1.4** Repeated experiments with varied relay hysteresis. The chosen hysteresis values are adequate for the solid Nyquist curve, but not for the dashed one.

shifts; from mechanical to analog, then to digital implementation. Over the years, more advanced control schemes have been introduced, but the PID controller is still the dominating choice in a multitude of applications. Several such applications are found in the regulatory layer of process industrial plants. From a control engineering perspective, a process industrial plant can be hierarchically organized according to Fig. 1.6 [Skogestad, 2004]. The top layers are controlled over longer time spans (weeks, days) and the decisions within them are more strategic than operational. The 'processes' within these layers are generally too complex to be handled by a PID controller. It is instead at the supervisory and regulatory control layers that the PID controllers are found.

A typical process industrial plant can contain thousands of PID loops. Their purpose is often to regulate a process with relatively simple input–output dynamics  $G_{u,y}$ , so that the closed-loop system from reference to output can be regarded as  $G_{r,y}(s) \approx 1$  by the next higher level in the hierarchy. Typical examples include level control in buffer tanks, temperature control in vessels and flow control in pipes. Set-point changes are rare, and the objective of the control is therefore commonly that of disturbance rejection.

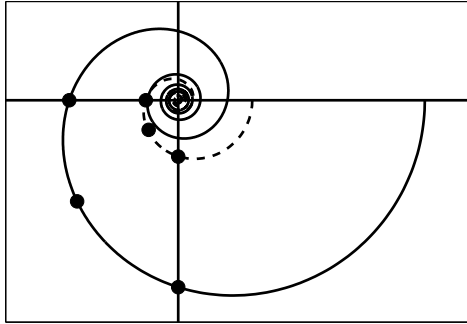


**Figure 1.5** Repeated experiments identifying points on the Nyquist curve at given phase angles of  $-90^\circ$ ,  $-135^\circ$  and  $-180^\circ$ .

Today approximately 95% of regulatory control loops in process industry utilize PI(D) control [Åström, 2002]. Most of these use PI controllers. In some cases, the phase lead associated with derivative action could increase performance significantly [Panagopoulos, 2000]. A plausible explanation to why derivative action is not used in these cases is that it makes it somewhat more demanding to arrive at an adequate controller tuning.

Despite the fact that PID control is an old and mature technology, several process industrial field reports indicate surprisingly low performance. The following results for PID control loop performance are adopted from [Ender, 1993]:

- $> 30\%$  operate in manual mode
- $> 30\%$  increase output variability
- $\approx 25\%$  use factory default parameters

A similar, but smaller, study [Bialkowski, 1993] gives the following numbers for PID control loops within process industry:

- 80% increase output variability
- 30% cycle due to poor tuning

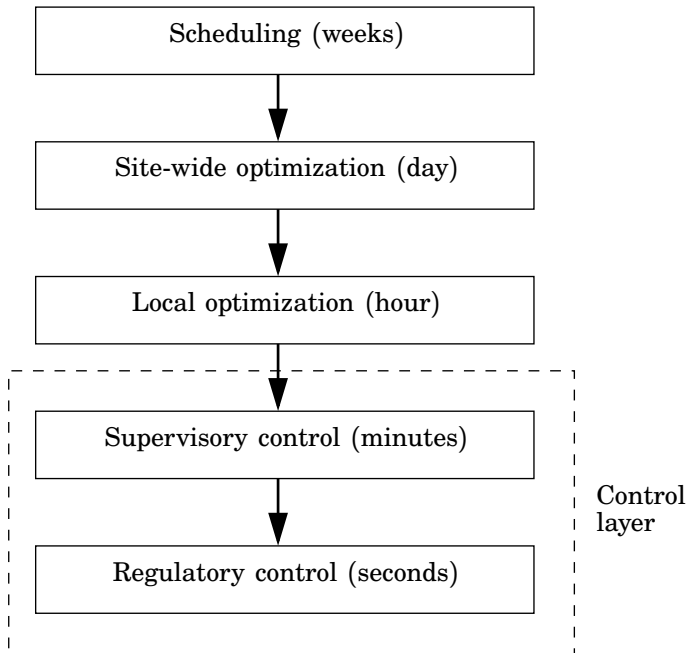


**Figure 1.6** Functional hierarchy of a process industrial plant.

Both surveys show that a significant fraction of PID loops in process industry have higher output variability in closed-loop operation, than in manual mode. The perhaps predominant reason for this situation is the time and money associated with adequately tuning a PID control loop. A survey by Honeywell, [Desborough and Miller, 2002], estimated the work cost alone to be USD 250 – 1000, per control loop. The above mentioned tuning situation combined with the relatively high cost of tuning a control loop motivates looking into fully automated tuning procedures, requiring no, or little, human interaction.

### **PID in Closed-Loop Anesthesia**

Clinical anesthesia can be divided into three components, as shown in Fig. 1.7. The role of hypnosis is to prevent unintended intra-operative

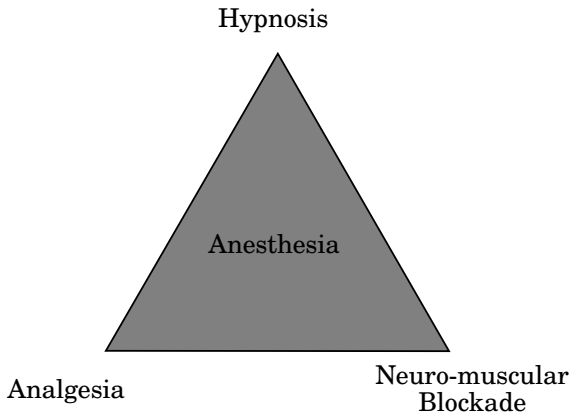


**Figure 1.7** Functional components of anesthesia.

awareness. In addition to this, it is essential to preserve a stable suppression of noxious stimulation of the circulatory and hormonal systems. This is the role of analgesia. Finally, in some cases local muscle relaxation is needed in order to successfully perform the surgery. Anesthetic drugs are categorized according to their effect; hypnotic, analgesic and neuro-muscular blocking agents [Bibian *et al.*, 2005]. The dose-effect dynamics of these agents are not independent. Especially, there exist a synergetic coupling between certain hypnotic and analgesic agents [Kern *et al.*, 2004], [Ferreira *et al.*, 2006].

During general surgery anesthesia is traditionally provided by an anesthesiologist, who manually doses the drugs guided by online measurable signals (such as heart rate, blood pressure and blood plasma oxygen saturation) and signs (e.g. response to various stimuli and spontaneous patient movement). The anesthesiologist hence acts as a fairly complex feedback controller. In addition, it is common to proactively dose anesthetic agents prior to foreseeable events such as increased surgical stimulation. There is hence also a feed forward path to the control signal.

With the availability of pharmacokinetic models, dynamically relating drug dose to effect site concentration, and pharmacodynamic models, relating effect site concentration to clinical effect, it is possible to predict the time evolution of the clinical effect, given the drug

infusion rate. An overview is found in [Bibian, 2006]. In order to limit model error the parameters of most pharmacokinetic (and some pharmacodynamic) models are related to demographic covariates such as body mass, length, sex and age. The predictability of dose–response has been developed into commercially available dosing regimens known as target controlled infusion, TCI [Glen, 1998]. In TCI the predicted effect is used to alter the current infusion rate. As any open loop strategy, TCI is sensitive to model error and disturbances. The anesthetist is still needed to counteract disturbances, which are mainly caused by the surgery, and to resolve any complications which lie outside the scope of the control system.

A natural extension of TCI would be to close a feedback loop from measured clinical effect. This would decrease sensitivity towards model error and disturbances. In this work attention is directed to controlling the depth of hypnosis (DOH), using propofol as the hypnotic agent. Surgical stimulation, typically lowering DOH, can be regarded as an output disturbance. Other system disturbances are measurement noise and load disturbances caused by the interaction with other anesthetic agents.

A principal challenge in controlling DOH lies in the availability of an adequate clinical measurement. Such a signal should at least be continuously available and monotonically increasing with the clinical effect. Although several signals (such as blood plasma oxygen saturation and respiratory rate) are correlated with DOH, it was not until the advent of measurements based on spectrum analysis methods applied to brain waves (EEG), that a calibrated signal with sufficiently high signal to noise ratio was available. There exist several commercial monitors for EEG based DOH measurement, including the bispectral index (BIS) [Liu *et al.*, 1997], entropy [Viertö-Oja *et al.*, 2004] and a wavelet based [Zikov *et al.*, 2006] monitor. The wavelet based monitor, NeuroSense NS-701 by NeuroWave, Cleveland, USA, has the advantage that its dynamics are well-approximated by a linear time invariant system, with transfer function coefficients published by its inventor.

Clinical studies in which DOH was controlled using propofol as anesthetic agent, an EEG based measurement signal and a PID controller have been conducted in the past [Absalom *et al.*, 2002], [Liu *et al.*, 2005]. The author is involved in a project where this setting is clinically evaluated within pediatrics at the British Columbia Chil-

dren's Hospital, Vancouver, Canada, where an initial pilot study involving 20 patients was successfully completed in September 2011.

The inter-patient variability in sensitivity to propofol is not fully captured by the demographic covariate-based pharmacokinetic and pharmacodynamic models [Schüttler and Ihmsen, 2000]. It would therefore be desirable to individualize controller tuning beyond what the published models enable. One possible way to do this would be to 1) record the DOH measurement during the transition from awake to an adequately sedated state together with the corresponding propofol infusion profile and 2) base the PID controller tuning on this response. In this approach, it is natural to address several concepts from the automatic PID tuning framework.

# 2

## Synopsis

### 2.1 Contributions

The work in this licentiate thesis is based on three publications. They are listed below, together with an explanation of their contribution to the thesis and the role of the author in the work behind each publication.

#### Paper I

Soltesz, K. and T. Hägglund (2011): “Extending the relay feedback experiment.” In *Proc. IFAC World Congress*. Milan, Italy.

The paper addresses the problem of devising an adequate system identification input signal, to be used in a PID auto-tuning scheme. The proposed method is an extension of the classic relay feedback experiment. It utilizes feedback over nonlinearities to excite the process dynamics around given phase angles. In a second stage, the signal is extended in an iterative fashion, to form a desired input power spectrum for a given phase range of the process dynamics. The feasibility of the method is demonstrated through a batch of simulations and one experiment using a physical process.

K. Soltesz developed the method and evaluated it in simulations and a laboratory experiment. T. Hägglund assisted in method development and with structuring the manuscript.

## Paper II

Soltesz, K., K. J. Åström, and T. Hägglund (2010): “Transfer function parameter identification by modified relay feedback.” In *Proc. American Control Conference*. Baltimore, USA.

Paper I dealt with experiment design for the PID auto-tuner. In this paper, a method for obtaining FOTD, and possibly SOTD, models from the sampled input–output pairs from the experiment, is presented. It is based on computing sensitivity derivatives of the output error, with respect to the parameters to be identified. A Newton-Raphson type search is subsequently used to find a parameter set (locally) minimizing the output error. The method is demonstrated through simulation on a batch of process models, which are representative for process industry applications.

K. Soltesz developed the method and conducted the simulations experiments. K. J. Åström provided the original idea behind the work. T. Hägglund helped in developing the method and assisted with structuring and editing the manuscript.

## Paper III

Soltesz, K., J.-O. Hahn, G. A. Dumont, and J. M. Ansermino (2011): “Individualized PID control of depth of anesthesia based on patient model identification during the induction phase of anesthesia.” In *Proc. IEEE Conference on Decision and Control and European Control Conference*. Orlando, USA.

Paper I and Paper II dealt with automatically obtaining low order process models for PID tuning, in situations where little a priori information is available. This paper targets a medical application where PID control and automatic tuning of the PID controller are useful. By measuring brain wave (EEG) activity of a patient under anesthesia, it is possible to estimate the anesthetic state. Based on this online measurement and a dynamical model of the patient, the anesthetic drug can then be administered in a closed-loop fashion. This paper investigates the possibility of individualizing (i.e., re-tuning) a drug delivery PID controller given the initial patient response. The method of Paper II is used to refine a process model estimate, based on which an individualized controller is tuned. A pilot version of the method is

demonstrated in simulation. In order to extend this version to a clinically adequate scheme further work is needed. Especially, robustness towards measurement noise and sufficient input excitation need to be ensured.

Currently, the authors (except J.-O. Hahn) are involved in a project where PID controlled closed-loop anesthesia is clinically evaluated. The controller is not yet individualized beyond what is possible with demographic covariates.

K. Soltesz did the simulations experiment. J.-O. Hahn provided the adequate background and assisted in structuring and editing the manuscript. G. A. Dumont coordinated the work and accommodated the original idea. J. M. Ansermino gave feedback on clinically related aspects.

### Other Publications

Apart from the publications within this thesis, the author has authored or co-authored the following publications, within the scope of PhD studies.

Linderoth, M., K. Soltesz, A. Robertsson, and R. Johansson (2011): “Initialization of the Kalman filter without assumptions on the initial state.” In *IEEE International Conference on Robotics and Automation (ICRA)*. Shanghai, China.

Soltesz, K., J.-O. Hahn, T. Hägglund, G. A. Dumont, and J. M. Ansermino (2011a): “Individualized closed-loop control of propofol anesthesia: A preliminary study.” *Transactions on Biomedical Engineering, IEEE*, September. Submitted.

Soltesz, K., C. Johnsson, and T. Hägglund (2011b): “Teaching control principles to industry practitioners.” In *Proc. SEFI Annual Conference*. Lisbon, Portugal.

# References

This is the bibliography of Chapter 1 and Chapter 2. Bibliographies of the individual contributions are found at the end of each corresponding paper re-print.

Absalom, A., N. Sutcliffe, and G. Kenny (2002): “Closed-loop control of anesthesia using bispectral index.” *Anesthesiology*, **96:1**, pp. 67–73.

Åström, K. J. (2002): “Control system design.”  
<http://www.cds.caltech.edu/~murray/courses/cds101/fa02/caltech/astrom.html> Version: October 4, 2011.

Åström, K. J. and T. Häggglund (1984): “Automatic tuning of simple regulators with specifications on phase and amplitude margins.” *Automatica*, **20:5**, pp. 645–651.

Åström, K. J. and B. Wittenmark (1996): *Computer Controlled Systems*. Prentice Hall.

Bialkowski, W. L. (1993): “Dream versus reality: A view from both sides of the gap.” *Pulp & Paper Canada*, **94:11**, pp. 19–27.

Bibian, S. (2006): *Automation in clinical anesthesia*. PhD thesis, University of British Columbia, Department of Electrical and Computer Engineering, Vancouver, Canada.

Bibian, S., C. R. Ries, M. Huzmezan, and G. Dumont (2005): “Introduction to automated drug delivery in clinical anesthesia.” *European Journal of Control*, **11:6**, pp. 535 – 537.

Desborough, L. and R. Miller (2002): “Increasing customer value of industrial control performance monitoring – Honeywell’s experience.” *AiChe Symposium Series*, **326**, pp. 169–189.

- Ender, D. B. (1993): "Process control performance: Not as good as you think." *Control Engineering*, **40:2**, pp. 180–190.
- Ferreira, D. A., C. S. Nunes, L. M. Antunes, I. A. Santos, F. Lobo, M. Casal, L. Ferreira, and P. Amorim (2006): "The effect of a remifentanil bolus on the bispectral index of the EEG (BIS) in anaesthetized patients independently from intubation and surgical stimuli." *European Journal of Anaesthesiology*, **23:4**, pp. 305–310.
- Friman, M. and K. V. Waller (1997): "A two-channel relay for autotuning." *Industrial and Engineering Chemistry Research*, **36:7**, pp. 2662–2671.
- Garpinger, O. and T. Hägglund (2008): "A software tool for robust PID design." In *Proc. 17th IFAC World Congress*. Seoul, Korea.
- Glen, J. B. (1998): "The development of Diprifusor: a TCI system for propofol." *Anesthesia*, **53**, pp. 13 – 21.
- Hägglund, T. and K. J. Åström (2002): "Revisiting the Ziegler-Nichols tuning rules for PI control." *Asian Journal of Control*, **4:4**, pp. 364–380.
- Johansson, K. H., A. E. Barabanov, and K. J. Åström (2002): "Limit cycles with chattering in relay feedback systems." *IEEE transactions on Automatic Control*, **47:9**, pp. 1414–1423.
- Kern, S. E., X. Guoming, J. L. White, and T. D. Egan (2004): "Opioid-hypnotic synergy: a response surface analysis of propofol-remifentanil pharmacodynamic interaction in volunteers." *Anesthesiology*, **100:6**, pp. 1374 – 1381.
- Lin, C., Q.-G. Wang, and T. H. Lee (2004): "Relay feedback: A complete analysis for first-order systems." *Industrial and Engineering Chemistry Research*, **43:26**, pp. 8400–8402.
- Liu, J., H. Singh, and P. White (1997): "Electroencephalographic bispectral index correlates with intraoperative recall and depth of propofol-induced sedation." *Anesthesia and Analgesia*, **84**, pp. 185 – 189.
- Liu, N., A. Genty, T. Chazot, and M. Fischler (2005): "Titration of propofol guided by bispectral index (bis): Closed-loop versus manual

## References

- target controlled infusion.” In *Proc. American Anesthesiology Society Conference*. Atlanta, USA.
- Panagopoulos, H. (2000): *PID-Control. Design, Extension, Application*. PhD thesis ISRN LUTFD2/TFRT--1059--SE, Department of Automatic Control, Lund University, Sweden.
- Schüttler, J. and H. Ihmsen (2000): “Population pharmacokinetics of propofol: A multicenter study.” *Anesthesiology*, **92:3**, pp. 727–738.
- Skogestad, S. (2003): “Simple analytic rules for model reduction and PID tuning.” *Journal of Process Control*, **13:4**, pp. 291–309.
- Skogestad, S. (2004): “Control structure design for complete chemical plants.” *Computers & Chemical Engineering*, **28:1-2**, pp. 219–234.
- Viertö-Oja, H., V. Maja, M. Särkelä, P. Talja, N. Tenkanen, H. Tolvanen-Laakso, M. Paloheimo, A. Vakkuri, A. Yli-Hankala, and P. Meriläinen (2004): “Description of the entropy algorithm as applied in the datex-ohmeda s/5 entropy module.” *Acta Anaesthesiol Scandinavica*, **48:2**, pp. 154–161.
- Ziegler, J. G. and N. B. Nichols (1942): “Optimum settings for automatic controllers.” *Transaction fo the ASME*, **64**, pp. 759–768.
- Zikov, T., S. Bibian, G. Dumont, M. Huzmezan, and C. Ries (2006): “Quantifying cortical activity during general anesthesia using wavelet analysis.” *IEEE Transactions on Biomedical Engineering*, **53:4**, pp. 617–632.

# Paper I

## **Extending the Relay Feedback Experiment**

**Kristian Soltesz   Tore Hägglund**

### **Abstract**

An augmented version of the traditional relay feedback experiment is proposed. It aims at producing an input with energy concentrated to a frequency band, corresponding to a certain phase sector of the Nyquist curve of the process to be identified. A non-convex problem is formulated. Sub-optimal, but efficient, algorithms are developed.

©2011 IFAC. Reprinted, with permission, from *Proceedings of the 18<sup>th</sup> IFAC World Congress*. Milan, Italy, 2011. The article has been modified to fit the current format. Discovered typographical errors have been corrected in this reprint.

## 1. Introduction

### 1.1 The Role of the Input Spectrum

When performing frequency domain system identification, it is well-known that higher spectral content (magnitude) of a certain frequency in the input generally yields better model accuracy of the obtained model around that frequency. To motivate this, consider estimation of LTI parameters  $\theta = [\mathbf{b} \ \mathbf{a} \ L]^T$  ( $\mathbf{a} \in \mathbb{R}^n$ ,  $\mathbf{b} \in \mathbb{R}^n$ ,  $L \in \mathbb{R}_+$ ) of the strictly proper continuous time transfer function process model

$$P(s) = \frac{B(s)}{A(s)} e^{-Ls} = \frac{\sum_{j=1}^n b_j s^{n-j}}{s^n + \sum_{i=1}^n a_i s^{n-i}} e^{-Ls}, \quad (1)$$

from sampled input and output data  $u(kh)$ ,  $y(kh)$ ,  $k = 0, \dots, N-1$ , where  $h$  is the sampling period. One identification method, presented in [Soltesz *et al.*, 2010], is the minimization of the squared output error

$$J(\hat{\theta}) = \frac{1}{2} \int_{t_0}^{t_f} (\hat{y}(t) - y(t))^2 dt, \quad (2)$$

where  $y$  is the output of  $P$  generated by  $u$  while  $\hat{y}$  is the corresponding output of the model  $\hat{P}$ . The sampled equivalent of (2) is given by

$$J_h(\hat{\theta}) = \frac{1}{2} \sum_{j=0}^{N-1} (\hat{y}(kh) - y(kh))^2. \quad (3)$$

By Parseval's theorem, applied to the DFT of  $\hat{y} - y$ , (3) is equivalent to

$$J_h(\hat{\theta}) = \frac{1}{2} \sum_{j=0}^{N-1} |\Delta P(\omega_j)|^2 |U(\omega_j)|^2, \quad (4)$$

where  $\Delta P(\omega) = \hat{P}(i\omega) - P(i\omega)$ ,  $U$  is the  $N$ -point DFT of  $u$  and  $\omega_j = \frac{2\pi}{Nh} j$ .

From (4) it can be readily seen that the cost component associated with a certain frequency is proportional to the input power of that

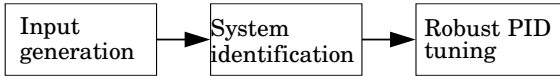


**Figure 1.** PID auto-tuning tool chain.

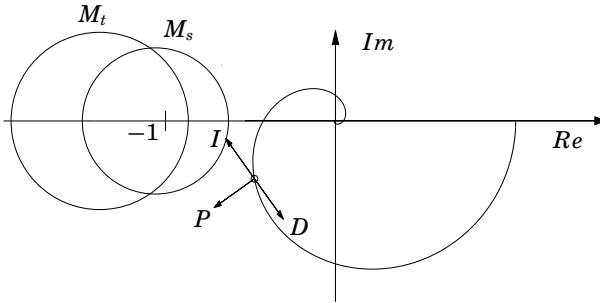


**Figure 2.** Nyquist curve interpretation of robust PID tuning.

frequency. It is therefore natural to ask what input spectrum should be chosen and how to synthesize the corresponding signal in the time domain. This paper addresses these questions in the context of system identification for PID tuning.

## 1.2 Input Spectrum for PID Tuning

The herein described input signal generation is intended to be the first link in a PID auto-tuning tool chain, outlined in Fig. 1.

Fig. 2 shows the Nyquist curve of a low pass, time delayed, process typical to process industry. The tuning of a PID controller can be interpreted as moving points of the process Nyquist curve by means of the P, I and D parts, according to the labeled arrows in Fig. 2, cf. [Åström and Hägglund, 2006].

Conventional methods for robust PID tuning, such as [Hägglund and Åström, 2002] and [Garpinger and Hägglund, 2008], ensure robustness by keeping the open loop transfer function outside a region surrounding  $-1$ . Avoiding the interior of the circles in Fig. 2 ensures sensitivity  $\|S\|_\infty < M_s$  and complementary sensitivity  $\|T\|_\infty < M_t$ .

Both the I and D parts introduce  $90^\circ$  phase shifts (in opposite directions). Hence it is desirable to have accurate models in different frequency regions, depending on which subclass of PID controller is synthesized. E.g., the model should be accurate around the negative real axis for P controllers, in the third quadrant for PI controllers and in the union of the second and third quadrant for PID controllers.

In this paper we will focus on the PI case, which is the industrially most common. The method can, however, be used for any combination of P, I and D. Hence, we seek an identification input with energy content concentrated to frequencies corresponding to the phase interval  $(-180^\circ, -90^\circ)$  of the process to be identified.

### 1.3 The Use of Relay Feedback

In [Åström *et al.*, 1995], it is concluded that stable, well damped LTI systems generally result in stable limit cycle oscillations, under relay feedback. A complete analysis for FOTD (first order plus time delay) systems is given in [Lin *et al.*, 2004]. According to describing function analysis, the fundamental harmonic of the oscillation occurs at the frequency  $\omega_{180}$ , corresponding to the phase  $\varphi = -180^\circ$  of the LTI system. This motivated the original relay feedback tuning method, [Åström and Hägglund, 1984]. Fig. 2.3(a) shows the experimental setup, with process  $P$  and nonlinearity  $N.L.$  Fig. 2.3(b) shows the input signal  $u_{a,180}$ , corresponding to 6 switches of the relay, with

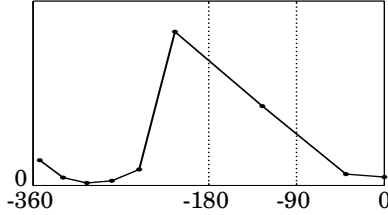
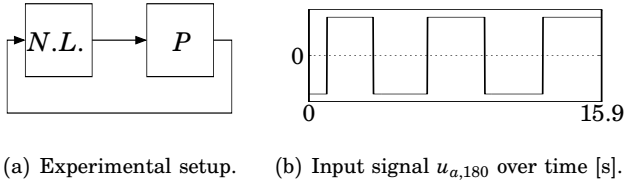
$$P(s) = \frac{1}{(s+1)(s+2)}e^{-s}. \quad (5)$$

The corresponding power spectrum, plotted against the phase frequencies of (5) is shown in Fig. 2.3(c). The vertical lines mark the frequencies corresponding to  $\varphi = -180^\circ$  and  $\varphi = -90^\circ$ .

As expected, energy is concentrated around  $\varphi = -180^\circ$ , rather than distributed over  $(-180^\circ, -90^\circ)$ , which would be desirable.

By introducing an integrator in the loop, the oscillation frequency is shifted to  $\varphi = -90^\circ$ ,  $\omega_{90}$ . Fig. 1 shows a nonlinearity described in [Friman and Waller, 1997], with describing function

$$N(a) = \frac{4h_p}{\pi a} - \frac{4h_i}{\pi a}i, \quad (6)$$



(c) Input power spectrum  $|U_{a,180}|^2$  over process phase  $\varphi$  [°].

**Figure 3.** Traditional relay experiment and corresponding input power spectrum.

corresponding to limit cycle oscillations at

$$\varphi = \arctan\left(\frac{h_i}{h_p}\right). \quad (7)$$

It may be used to shift the energy peak, but does not address the issue of energy distribution over a frequency interval.

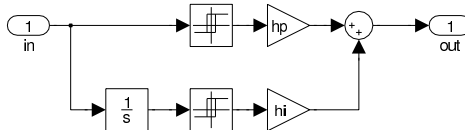


**Figure 4.** Two channel relay (Simulink implementation).

## 2. Problem formulation and Approach

We will now present the input design problem and investigate some approaches. The notation, used throughout the remainder of the paper, is introduced below.

### 2.1 Notation

Denote by  $U \triangleq Fu$  the DFT of  $u$  and by  $U_j$ ,  $j \in [0, \dots, N - 1]$  its  $j^{\text{th}}$  component. The DFT matrix  $F$  is defined through

$$F_{k,l} = \omega^{kl}, \quad \omega = e^{\frac{-2\pi i}{N}}. \quad (8)$$

Let

$$\omega_j = \frac{2\pi}{Nh}j, \quad a_j = |U_j|, \quad P_j = |U_j|^2, \quad \phi_j = \angle U_j \quad (9)$$

be the corresponding angular frequency, amplitude, power and phase respectively.

The sample operator associated with sample period  $h$  is

$$\mathbb{I}_h(t) = \sum_{k=-\infty}^{\infty} \delta(t - kh). \quad (10)$$

### 2.2 Two Stage Experiment

The aim is to obtain a power spectrum similar to that of Fig. 5 by extending the experiment of Fig. 2.3(a), while keeping experiment duration short and input power low.

A first step in this direction is obtained by conducting a two stage experiment, using the two channel relay. Stage one, yielding  $u_{a,180}$ , shown in Fig. 2.3(b), consists in 6 switches with  $h_p = 1$ ,  $h_i = 0$  ( $\varphi = -180^\circ$ ). Stage two, yielding  $u_{a,90}$ , consists in 4 switches with  $h_p = 0$ ,  $h_i = 1$  ( $\varphi = -90^\circ$ ) and is shown together with  $u_{a,180}$  in Fig. 2.6(a). The number of switches were empirically decided, based on experiments with  $P$ , commonly occurring in process industry and listed in [Hägglund and Åström, 2002]. In order to find the peak frequencies, the two sequences are individually normalized with respect to energy, forming

$$u'_a = \left[ \begin{array}{cc} u_{a,180} & u_{a,90} \\ u_{a,180}^T u_{a,180} & u_{a,90}^T u_{a,90} \end{array} \right]^T. \quad (11)$$

## 2. Problem formulation and Approach

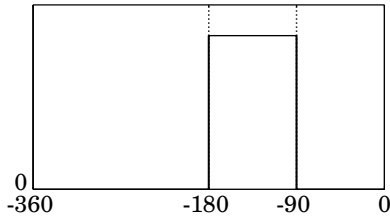
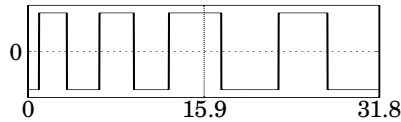
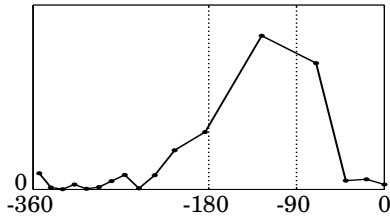


**Figure 5.** Reference input power spectrum  $Q$  over process phase  $\varphi$  [ $^\circ$ ].



(a) Input signal  $u_a$  over time [s].



(b) Input power spectrum  $|U'_a|^2$  over process phase  $\varphi$  [ $^\circ$ ].

**Figure 6.** Two stage relay experiment and corresponding (modified) input power spectrum.

The power spectrum  $|U'_a|^2$  is shown in Fig. 2.6(b). Two distinct peaks lie close to the frequencies corresponding to the desired phase angles. Experiments show that this is generally true for FOTD and SOTD (second order plus time delay) processes, which is indicated by results presented later in the paper.

The final stage consists in augmenting the experiment in order to obtain a magnitude spectrum similar to that of Fig. 5.

### 2.3 General Signal Augmentation Problem

An initial experiment has provided a zero order hold input sequence  $u_a = [u_{a,180}^T \ u_{a,90}^T]^T$  with sample period  $h$  and length  $N_a$ , as shown in Fig. 2.6(a). Using the power spectrum  $|U'_A|^2$ , the desired power spectrum  $Q$ , shown in Fig. 5, can be determined and approached by augmenting  $u_a$  with  $u_b$ , forming

$$u = \begin{bmatrix} u_a \\ u_b \end{bmatrix}. \quad (12)$$

Assuming fixed length  $N_b$  of  $u_b$ , we can formulate the synthesis problem

$$\min_{u_b} \underbrace{\left\| Q - \text{diag} \left( F \begin{bmatrix} u_a \\ u_b \end{bmatrix} \begin{bmatrix} u_a \\ u_b \end{bmatrix}^T F^* \right) \right\|_R}_{J(u)}, \quad (13)$$

where  $R$  is some vector norm. It is also natural to impose

$$\|u_b\|_\infty \leq \|u_a\|_\infty. \quad (14)$$

The problem, given by (13) is generally not convex in  $u_b$ , which can be deduced from e.g. the setup  $N_a = 0$ ,  $N_b = 2$ ,  $u_b = \begin{bmatrix} u_1 & u_2 \end{bmatrix}^T$ ,  $Q = 0$  and  $R = 2$  resulting in

$$\min_{u_1, u_2} \sqrt{2(u_1^4 + 6u_1^2u_2^2 + u_2^4)} \Leftrightarrow \min_{x_1, x_2} x_1^2 + 6x_1x_2 + x_2^2, \quad (15)$$

where the equivalence follows from the substitution  $x_1 = u_1^2$ ,  $x_2 = u_2^2$ . The eigenvalues of the objective Hessian are given by

$$\text{sp}(H(x_1^2 + 6x_1x_2 + x_2^2)) = \text{sp} \left( 2 \begin{bmatrix} 1 & 3 \\ 3 & 1 \end{bmatrix} \right) = \begin{bmatrix} -4 \\ 8 \end{bmatrix}. \quad (16)$$

(The objective is not convex, since its Hessian is indefinite.)

Further, there does generally not exist  $u_b$ , which bring the norm of (13) to 0. For instance, if  $u_a \neq 0$  and  $Q = 0$ , this would result in  $u_b$  of negative energy.

## 2.4 Particular Problem

Here, without further motivation, the norm  $R$  of (13) was chosen to be a weighted Euclidean norm. The weighting was chosen 1 for elements  $j \in I$  corresponding to frequencies  $\omega_j$  between the two peaks of  $|U_{a,180}|$  and  $|U_{a,90}|$  and 0 for all other elements. All elements of  $Q$  were chosen as  $\max_j |(U_a)_j|$ , corresponding to the flat energy spectrum in the third quadrant, shown in Fig. 5. For notational convenience, the sequence  $u_b$  was chosen to be of the same length as  $u_a$ , i.e.,  $N_a = N_b = N/2$ .

## 2.5 Optimization

We have not found any convexifications of (13), without introducing relaxations resulting in suboptimality. The proposed optimization strategy consists in two iterative stages. During the first stage, the error  $J(u_k)$  is monotonically non-increasing in the iterations  $k$ . The second stage lacks this property, but has shown good results in all experiments. The solution is chosen as

$$u_k^*, k^* = \arg \min_k J(u_k), \quad (17)$$

and is obtained either from the last iteration of stage one or any (usually among the last) iteration of stage two.

**Stage One** Each iteration of the algorithm consists in sorting the frequencies  $\omega_j$ , between the  $|U_{a,180}|$  and  $|U_{a,90}|$  peaks with respect to corresponding magnitude error. Starting with the  $w_j$  corresponding to the largest error, a sinusoid  $\Delta u_b$  in phase with the existing  $w_j$  component in  $u$  is added to  $u_b$ . The amplitude is chosen to minimize the norm in (13). If the norm cannot be decreased by  $\epsilon = 5\%$ ,  $\Delta u_b$  is discarded, and the next  $\omega_j$  from the sorted list is assessed. If the norm cannot be decreased by  $\epsilon$  for any  $\omega_j$ , stage one is terminated. Else, a new iteration is executed, now with  $u$  replaced by  $u + [0 \cdot u_a^T \Delta u_b^T]^T$ .

An algorithmic presentation is given in Algorithm 1. For notational convenience, we introduce

$$\Delta u_{0,b} = [0 \cdot u_a^T \Delta u_b^T]^T \quad (18)$$

and

$$W_b = \theta(N_a + 1) - \theta(N), \quad (19)$$

---

**Algorithm 1** Synthesis of  $u_b$ , stage one.

---

```

repeat
  flag = false
  queue = sortj |Qj - Pj|
  for all j in queue do
    Δu0,b = WbIIIh(t) cos(ωjt + φj)
    a = arg minj J(u + aΔu0,b)
    Δu0,b * = a
    if J(u + Δu0,b)/J(u) < 1 - ε then
      u = u + Δu0,b
      flag = true
    else
      flag = false
    break
  end if
end for
until not flag

```

---

where  $\theta(k)$  is the Heaviside step at  $k$ .

The problem of minimizing  $J$  over  $a$  is given by

$$\min_a \underbrace{\sum_{j \in I} |Q_j - |F_j(u + a\Delta u_{0,b})|^2}_{M_1(a)}, \quad (20)$$

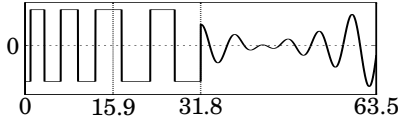
where  $M_1(\cdot)$  is a fourth order polynomial with known coefficient. Hence the solution of (20) is given by

$$\min_{a \in A} M(a), \quad A = \left\{ a; \frac{dM_1}{da} = 0 \right\}. \quad (21)$$

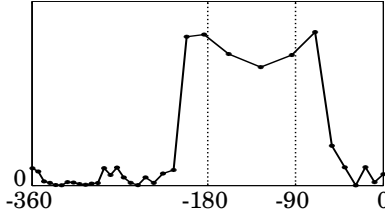
Fig. 2.7(a) shows the result, when the algorithm is applied to  $u$  from Fig. 2.6(a). The corresponding power spectrum is shown in Fig. 2.7(b).

**Stage Two** This stage is similar to stage one, but rather than minimizing the error norm, the magnitude error at  $\omega_j$  is brought to 0 in each iteration. Due to spectral leakage, however, the magnitude errors

## 2. Problem formulation and Approach



(a) Input  $u$  over time [s].



(b) Power spectrum  $|U|^2$  over process phase  $\varphi$  [°].

**Figure 7.** Input signal and corresponding power spectrum after first optimization stage.

at  $\omega_{l \neq j}$  might simultaneously increase. An algorithmic presentation is given in Algorithm 2.

---

**Algorithm 2** Synthesis of  $u_b$ , stage two.

---

**repeat**

$$j = \arg \min_j |Q_j - P_j|$$

$$\Delta u_{0,b} = W_b \text{III}_h(t) \cos(\omega_j t + \phi_j)$$

$$a = \arg \min_a |Q_j - |F_j(u + a\Delta u_{0,b})|^2|$$

$$u = u + a\Delta u_{0,b}$$

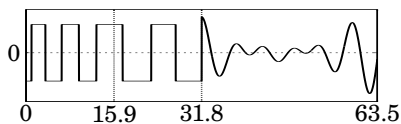
**until**  $|Q_j - P_j| < \epsilon$

---

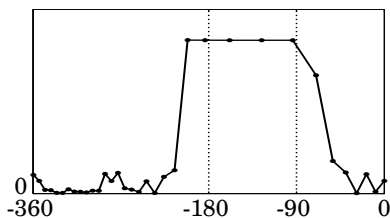
The minimization step is similar to that of Stage one, with (20) replaced by

$$\min_a \underbrace{|\sqrt{Q_j} - |F_j(u + a\Delta u_{0,b})||}_{M_2(a)}, \quad (22)$$

where  $M_2(\cdot)$  is a third order polynomial with known coefficients.



(a) Input  $u$  over time [s].



(b) Power spectrum  $|U|^2$  over process phase  $\varphi$  [°].

**Figure 8.** Input signal and corresponding power spectrum after second optimization stage.

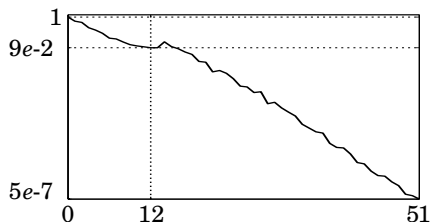


**Figure 9.** Normalized error  $J(u_k)/J(u_0)$  over optimization iterations  $k$ . Vertical line marks boundary between stage one and two. Logarithmic scale.

Fig. 2.8(a) and 2.8(b) correspond to Fig. 2.7(a) and 2.7(b). The error  $J(u_k)$  over iterations  $k$  is shown in log scale in Fig. 9. The vertical line indicates the boundary between stages one and two.

## 2.6 Practical Considerations

**Limiting Leakage** In addition to parametrizing  $u_b$  in sinusoids, with phases chosen to be consistent with  $u$ , one might consider various windows, to reduce spectral leakage. However, practical experience has shown that windowing does not contribute significantly to the convergence of the presented algorithms.

The amplitude constraint (14) can be incorporated in the algorithms by limiting  $|a|$  in each iteration, to a value where the constraints are met. Naturally, this imposes suboptimality. The level of suboptimality can be decreased by increasing the length of  $u_b$ ,  $N_b$ .

Depending on how the signal pair  $u, y$  will be used, one may or may not care about the magnitude spectrum outside the reference window. One way of avoiding spectral leakage from the optimization to form peaks at the edges of the window is to begin each optimization iteration by detecting the largest peak outside the window and add an out of phase sinusoid, reducing it to a tolerable value. This method was used when generating the results, presented below.

**Noise and Relay Hysteresis** It is not desirable to trigger subsequent relay switches at zero crossings, due to noise. A straight forward method for avoiding this is the introduction of hysteresis, which can be either in the signal magnitude or time domain. Here, signal magnitude is advantageous, since the time scale is unknown a priori.

**Adapting the Sample Period** Since the experiment duration is unknown a priori, the approach has been to introduce a buffer of fixed length  $N_a = 2^{10}$ . The system is then sampled with period  $h_0$  (as fast as the hardware allows) until the buffer is filled. The sample period is updated  $h_1 = 2h_0$  and every second sample is overwritten, corresponding to a down sampling of a factor 2. If the experiment is not completed when the end of the buffer is reached anew, the procedure is repeated with  $h_{k+1} = 2h_k$ .

**Meeting the Real-Time Constraint** Since the optimization needs to be conducted online, it starts executing at the second last switch of  $u_a$  in Fig. 2.6(a). Stage one is associated with a halting criterion, while stage two executes until the last switch of  $u_a$ . The time between the

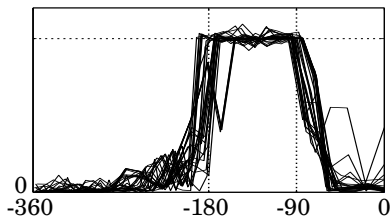


**Figure 10.** Power spectra  $|U|^2$  over process phase  $\varphi$  [ $^\circ$ ] for a FOTD and SOTD batch.

second last and last switch is assumed to be the same as that between the third and second last.

### 3. Simulation Results

The algorithms described above have been evaluated on a large set of FOTD and SOTD processes of the forms

$$P_1(s) = \frac{e^{-s}}{1 + sT_1}, \quad P_2(s) = \frac{e^{-s}}{(1 + sT_1)(1 + sT_2)}, \quad (23)$$

with varying  $T_k, k = 1, 2$  corresponding to normalized time delay in the range  $0.17 < \tau < 0.98$ .

Fig. 10 shows the power spectra (cf. Fig. 2.8(b)) resulting from applying the method to the batch. The spectra have been normalized w.r.t.  $Q$  in (13), to facilitate visualization. Algorithm 2 was limited to run  $k_{\max} = 100$  iterations.

### 4. Physical Example

Once the input has been applied to the system, the recorded input and output data is used to fit a FOTD or SOTD model. This is done in two stages. The first stage consists in obtaining initial parameters and deciding model order, using a vector-fitting approach, under current development. The second stage is a gradient based optimization,

described in [Soltesz *et al.*, 2010], minimizing

$$J(\theta) = \frac{1}{2} \int_{t_0}^{t_f} [y(t) - \hat{y}_\theta(t)]^2 dt, \quad (24)$$

where  $y$  is the recorded output and  $\hat{y}_\theta$  the output of a simulation using a transfer function parametrized in  $\theta$ .

Once the model is obtained, it is used as the basis for choosing PID parameters. The method of choice is one by [Garpinger and Hägglund, 2008], where the integrated absolute error (IAE) from a load step disturbance is minimized, subject to sensitivity, complementary sensitivity and control signal variance constraints, as outlined in (25). Cf. Fig. 2, where  $C$  is the transfer function of the PID controller.

$$\begin{aligned} \min_{K, T_i, T_d \in \mathbb{R}^+} & \int_0^\infty |e(t)| dt & (25) \\ \text{s.t.} & \\ |S(i\omega)| \leq M_s, & |T(i\omega)| \leq M_t, \forall \omega \in \mathbb{R}^+, \\ \|C(s)S(s)\|_2^2 = & \frac{\sigma_u^2}{\sigma_n^2} \leq V_k. \end{aligned}$$

Without going into further detail regarding the two last blocks of Fig. 1, the operation of the auto-tuner is demonstrated, using a lab scale tank process. A schematic sketch is shown in Fig. 2.11(a). Fig. 2.11(b) shows a photo of the actual process.

First principle modeling, [Bernoulli, 1738], yields the ODE

$$\frac{dh}{dt} = -\frac{a}{A} \sqrt{2gh} + \alpha u, \quad (26)$$

where  $h$  [m] is the (measured) water level,  $u \in (0, 1)$  is the input, proportional to the inflow through  $\alpha$  [ $\text{m}^3 \cdot \text{s}^{-1}$ ].  $l$  [ $\text{m}^3 \cdot \text{s}^{-1}$ ] is an uncontrolled and unmeasured disturbance flow.  $A$ ,  $a$  [ $\text{m}^2$ ] are the tank and outlet cross sections, respectively. The delay  $L$  [s] is due to the actuating pump and (intentionally) slow communications.

Linearizing around a nominal level  $h_0$  [m] and introducing  $y = \beta h \in (0, 1)$ , where  $\beta$  [ $\text{m}^{-1}$ ] is the sensor gain, an FOTD model is

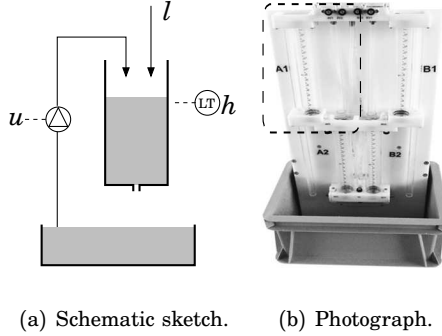


**Figure 11.** Tank process. Dashed region in photo marks sketch.

obtained:

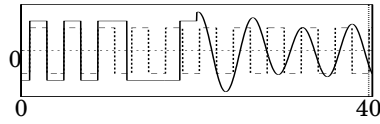
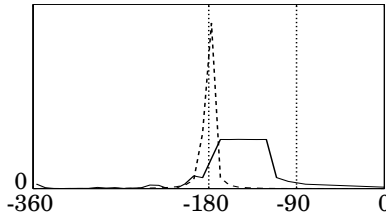
$$\Delta Y(s) = \frac{K e^{-sL}}{sT + 1} \Delta U(s), \quad K = \frac{\alpha}{a} \sqrt{\frac{2x_0\beta}{g}}, \quad T = \frac{A}{a} \sqrt{\frac{2x_0}{g\beta}}. \quad (27)$$

The  $\Delta$ :s denote deviation from the linearization point. Note however that the available signals are  $u, y$  rather than  $\Delta u, \Delta y$ . Also note that only non-negative inflow is possible, i.e.,  $\alpha = 0$  when  $u < 0$ .

Fig. 2.12(a) shows the input signal generated by the proposed method together with that of a traditional relay experiment. The signals are of equal duration and energy. The corresponding power spectra are shown in Fig. 2.12(b). Here process phase is that obtained when inserting numerical measurement values of  $a, A, \alpha, \beta, h_0, L$  into (3).

From Fig. 2.12(a) it is obvious that fitting the three FOTD parameters to the input-output data of the traditional relay comes with numerical difficulty, since virtually all energy is concentrated to a narrow spectral peak, yielding only one complex number, i.e., two parameters.

Based on the input-output data from the extended relay experiment, PI parameters were obtained using [Garpinger and Hägglund, 2008] with  $M_s = M_t = 1.4, V_k = 4$ . Fig. 2.13(a) shows the plant output of experiments where a reference step from  $r = 0.8h_0$  to  $h_0$  occurred at  $t = 5$  s, followed by a load step at  $t = 30$  s. At  $t = 70$  s, white zero mean measurement noise, with variance 0.005, was added. Fig. 2.13(b) shows the corresponding  $u$ .

(a) Input signal  $u_a$  over time [s].(b) Input power spectrum  $|U'_a|^2$  over process phase  $\varphi$  [°].

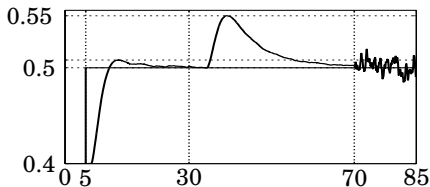
**Figure 12.** Input signal and corresponding power spectrum from tank experiment. Relay (dashed), extended (solid).

## 5. Conclusion

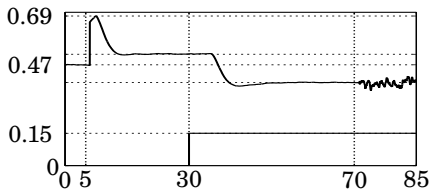
The paper addresses the problem of input magnitude spectrum shaping, in the context of PID auto-tuning.

A two stage optimization method, for magnitude spectrum shaping was presented and demonstrated. It shows satisfactory result for the class of processes (FOTD and SOTD) interesting from a PID tuning perspective.

The algorithm was applied to physical data and the auto-tuning procedure, of which the algorithm is a part, was outlined and demonstrated.



(a) Ref.  $r$  and output  $y$  over time [s].



(b) Input  $u$  and load  $l$  over time [s].

**Figure 13.** Closed loop response to reference step, load step and measurement noise. (There is a 5 s transport delay on the disturbance step, due to the hardware.)

## 6. Future Work

A natural question is if the problem formulation (13) can be relaxed into a convex program (without introducing suboptimality). It is also of interest to see if this can be done when the second part,  $u_b$ , of the input is constrained according to (14), which defines a convex region.

From a signal generation perspective it would be even more beneficial if  $u_b$  was only allowed to take binary values  $\in \{u_{\min}, u_{\max}\}$ , as is the case for  $u_a$ . This results in a binary program of high dimensionality, which is not tractable without further reformulation or relaxation.

It is desirable to choose magnitude  $\|u_a\|_\infty$ , resulting in  $c_l \cdot \sigma_n < \|y_a\|_\infty < c_h \sigma_n$ , where  $\sigma_n$  is the standard deviation of the output  $y_a$  due to measurement noise.  $c_l \approx 1$  and  $c_h \approx 2$  are constants. This is a feedback problem, since the process gain is unknown before the experiment.

In addition, several issues concerning the two rightmost blocks in Fig. 1, remain to be addressed before the PID tuning chain functions reliably enough for industrial use.

## References

- Åström, K. J., G. C. Goodwin, and P. R. Kumar (1995): *Adaptive Control, Filtering and Signal Processing*. Springer-Verlag.
- Åström, K. J. and T. Hägglund (1984): “Automatic tuning of simple regulators with specifications on phase and amplitude margins.” *Automatica*, **20:5**, pp. 645–651.
- Åström, K. J. and T. Hägglund (2006): *Advanced PID Control*. ISA.
- Bernoulli, D. (1738): *Hydrodynamica*.
- Friman, M. and K. V. Waller (1997): “A two-channel relay for autotuning.” *Industrial and Engineering Chemistry Research*, **36:7**, pp. 2662–2671.
- Garpinger, O. and T. Hägglund (2008): “A software tool for robust PID design.” In *Proc. 17th IFAC World Congress*. Seoul, Korea.
- Hägglund, T. and K. J. Åström (2002): “Revisiting the Ziegler-Nichols tuning rules for PI control.” *Asian Journal of Control*, **4:4**, pp. 364–380.
- Lin, C., Q.-G. Wang, and T. H. Lee (2004): “Relay feedback: A complete analysis for first-order systems.” *Industrial and Engineering Chemistry Research*, **43:26**, pp. 8400–8402.
- Soltész, K., K. J. Åström, and T. Hägglund (2010): “Transfer function parameter identification by modified relay feedback.” In *Proc. American Control Conference*. Baltimore, USA.

# Paper II

## **Transfer Function Parameter Identification by Modified Relay Feedback**

**Kristian Soltesz   Tore Hägglund  
Karl Johan Åström**

### **Abstract**

This paper proposes a method of finding low order models of a SISO transfer function based on relay feedback. Parameter identification is posed as a (non-convex) squared output error minimization problem, numerically solved utilizing Newton-Raphson iteration with back tracking line search. Focus lies on computing the cost function gradient and Hessian with respect to the parameter vector and on finding a feasible starting point. The method is demonstrated for FOTD model identification. A modified relay method is used to ensure good excitation around a predefined phase angle for the system. The method requires no a priori system information. The identification method is evaluated on a batch of common process industry processes. Finally, conclusions and suggestions on future work are provided.

©2010 IFAC/AACC. Reprinted, with permission, from *Proceedings of the 2010 American Control Conference*. Baltimore, USA, 2010. The article has been modified to fit the current format. Discovered typographical errors have been corrected in this reprint.

## 1. Introduction

The use of relay feedback [Åström and Hägglund, 1984] as process identification method has been around for a long time. Its main application has been in automatic tuning of PID controllers in process industry, where it is still broadly used, due to its simplicity and reliability.

The original method yields the point on the Nyquist curve corresponding to the phase crossover frequency. The method has been augmented with various modifications of the relay non-linearity, [Friman and Waller, 1997] being one of the more elegant, resulting in the possibility to identify a point on the Nyquist curve other than that corresponding to the phase crossover frequency.

Several alternative data analysis methods have been proposed. Mats Lilja utilized least square regression to identify low order time delayed transfer function models from frequency domain data (i.e. several points on the Nyquist curve) [Lilja, 1988].

Here an optimization method, yielding a transfer function description of the process to be identified, is presented. A discrete time counterpart of the method is outlined in [Åström and Bohlin, 1965]. The method is based on Newton-Raphson iteration over a cost function of the transfer function parameters. Cost derivatives (Jacobian and approximation of Hessian) are obtained through simulation of an augmented system. Due to non-convexity of the cost function in the transfer function parameters, a close-to optimal initial parameter guess is desirable. Such initial guess has here been obtained by gridding the normalized time delay of the model, evaluating the cost for each grid point, and choosing the parameters corresponding to the minimum as starting point for the optimization.

Input signals generated through a modified relay feedback are considered, since it allows for signal energy concentration around a frequency corresponding to a pre-defined phase lag of the system to be identified, without a priori system information. For PI(D) tuning applications, a frequency corresponding to a point in the third quadrant of the Nyquist curve is preferable. Since PI provides a phase lag, the obtained model needs not be accurate for phase lags larger than  $145^\circ$ , whereas accuracy up to the phase crossover frequency can be of interest when considering PID control, due to the phase lead of the controller [Åström and Hägglund, 2006].

In order to verify generality of the method, it has been tested on the AMIGO<sup>1</sup> batch, consisting of nine classes of processes, cf. [Åström and Hägglund, 2006]. Per design, the process models of the batch are representative for process control industry, which is also the main target application field of the material which follows.

## 2. Optimization Method for Identification

Here the proposed identification method is presented. Time is assumed to be continuous.

### 2.1 Objective

Our aim is to identify parameters  $\theta = [\mathbf{b} \ \mathbf{a} \ L]^T$  ( $\mathbf{a} \in \mathbb{R}^n$ ,  $\mathbf{b} \in \mathbb{R}^n$ ,  $L \in \mathbb{R}_+$ ) of the time delayed strictly proper continuous time transfer function process model

$$P(s) = \frac{B(s)}{A(s)} e^{-Ls} = \frac{\sum_{j=1}^n b_j s^{n-j}}{s^n + \sum_{i=1}^n a_i s^{n-i}} e^{-Ls}. \quad (1)$$

If the number of zeros is believed to be  $m < n - 1$ , we assign  $b_1 = \dots = b_{n-m-1} = 0$ . Given input sequence  $u(t)$  and corresponding output sequence  $y(t)$ , we formulate the objective as to minimize the mean squared output error

$$J(\hat{\theta}) = \frac{1}{2} \int_{t_0}^{t_f} (\hat{y}(t) - y(t))^2 dt, \quad (2)$$

where

$$\hat{y}(t) \triangleq \mathcal{L}^{-1}(\hat{P}(s)) \cdot U(s). \quad (3)$$

The problem is convex in  $\hat{\mathbf{b}}$  and  $\hat{L}$ . However, it is non-convex in  $\hat{\mathbf{a}}$ . For example, letting the model be defined through  $\hat{\theta} = [\hat{a}_1 \ \hat{a}_2 \ \hat{a}_3 \ 0 \ 0 \ \hat{b}_3 \ \hat{L}]^T$  and freezing all parameters except  $\hat{a}_3$  according to  $\hat{\theta} = [1 \ 0 \ \hat{a}_3 \ 0 \ 0 \ 1 \ 0]^T$  yields

$$J(\hat{\theta}) = \frac{1}{2} \int_0^1 \mathcal{L}^{-1}(\hat{P}(s)^2) = \frac{1}{2} \int_0^1 \sin(\hat{a}_3 t)^2 dt$$

---

<sup>1</sup>AMIGO stands for Approximate M-constrained Integral Gain Optimization. The AMIGO test batch was originally used to obtain guidelines for a Ziegler-Nicholes type tuning scheme.

which is clearly not convex in  $\hat{a}_3$ .

## 2.2 Newton-Raphson Method

Due to the general non-convexity of (2) there exists no known method, guaranteeing convergence to the global minimum. A candidate method, which has proved successful for the problem instances we have analyzed, has been the Newton-Raphson approach, involving the computation of  $\nabla J(\hat{\theta})$  and  $\nabla^2 J(\hat{\theta})$  in each iteration.

## 2.3 Evaluation of Gradient

The gradient is given by

$$\nabla J(\hat{\theta}) = \int_{t_0}^{t_f} \frac{\partial}{\partial \hat{\theta}} \frac{1}{2} (\hat{y} - y)^2 dt = \int_{t_0}^{t_f} (\hat{y} - y) \frac{\partial \hat{y}}{\partial \hat{\theta}} dt. \quad (4)$$

Introducing the canonical controllable state space form of  $\hat{P}(s)$  yields

$$\frac{\partial \hat{\mathbf{x}}}{\partial t} = \hat{\mathbf{A}} \hat{\mathbf{x}} + \hat{\mathbf{B}} u \quad (5)$$

$$\hat{y} = \hat{\mathbf{C}} \hat{\mathbf{x}}, \quad (6)$$

where

$$\frac{\partial \hat{x}_1}{\partial t} = -\hat{\mathbf{a}}^T \hat{\mathbf{x}} + u \quad (7)$$

$$\frac{\partial \hat{x}_k}{\partial t} = \hat{x}_{k-1}, \quad 2 \leq k \leq n \quad (8)$$

$$\hat{y} = \hat{\mathbf{b}}^T \hat{\mathbf{x}}. \quad (9)$$

In order to calculate  $\nabla J(\hat{\theta})$ , we need to evaluate

$$\frac{\partial \hat{y}}{\partial \hat{\theta}} = \mathbf{C} \frac{\partial \hat{\mathbf{x}}}{\partial \hat{\theta}}. \quad (10)$$

From (9) we obtain

$$\frac{\partial \hat{y}}{\partial \hat{b}_k} = \hat{x}_k, \quad 1 \leq k \leq n. \quad (11)$$

## 2. Optimization Method for Identification

Finding partial derivatives of  $\hat{y}$  w.r.t. the components of  $\hat{\mathbf{a}}$  is somewhat more involving. From (3) we obtain

$$\hat{Y}(s) = \frac{\hat{B}(s)}{\hat{A}(s)} e^{-\hat{L}s} U(s) \Rightarrow \quad (12)$$

$$\Rightarrow \frac{\partial \hat{Y}(s)}{\partial \hat{a}_k} = -\frac{s^{n-k}}{\hat{A}(s)} \hat{Y}(s), \quad 1 \leq k \leq n \quad (13)$$

The dynamics of (13) can be incorporated in the state space description (5), (6) by augmenting  $n$  states  $\hat{\mathbf{z}}$  to the state vector  $\hat{\mathbf{x}}$ , forming  $\hat{\mathbf{x}}_e = [\hat{\mathbf{x}}^T \hat{\mathbf{z}}^T]^T$ . Letting the augmented states take on the roles

$$\hat{z}_k = -\frac{\partial \hat{y}}{\partial \hat{a}_k}, \quad 1 \leq k \leq n \quad (14)$$

we utilize (13) to obtain the augmented state dynamics

$$\frac{\partial \hat{z}_1}{\partial t} = \hat{y} - \hat{\mathbf{a}}^T \hat{\mathbf{z}} = \hat{\mathbf{b}}^T \hat{\mathbf{x}} - \hat{\mathbf{a}}^T \hat{\mathbf{z}} \quad (15)$$

$$\frac{\partial \hat{z}_k}{\partial t} = \hat{z}_{k-1}, \quad 2 \leq k \leq n. \quad (16)$$

The augmented system in  $\hat{\mathbf{x}}_e$  provides the desired parameter derivatives

$$\hat{y} = \hat{\mathbf{b}}^T \hat{\mathbf{x}} \quad (17)$$

$$\frac{\partial \hat{y}}{\partial \hat{\mathbf{b}}} = \mathbf{I}_n \hat{\mathbf{x}} \quad (18)$$

$$\frac{\partial \hat{y}}{\partial \hat{\mathbf{a}}} = -\mathbf{I}_n \hat{\mathbf{z}}. \quad (19)$$

Finally, from (1), we obtain

$$\frac{\partial \hat{Y}(s)}{\partial \hat{L}} = -s \frac{\hat{B}(s)}{\hat{A}(s)} e^{-\hat{L}s} U(s). \quad (20)$$

Using (7)-(9) the parameter derivative can be written

$$\frac{\partial \hat{y}}{\partial \hat{L}} = \hat{a}_n \hat{b}_1 \hat{x}_n - \hat{b}_1 u + \sum_{j=1}^{n-1} (\hat{a}_j \hat{b}_1 - \hat{b}_{j+1}) \hat{x}_j. \quad (21)$$

## 2.4 Hessian Approximation

The Hessian of (2) is given by

$$\nabla^2 J(\hat{\boldsymbol{\theta}}) = \int_{t_0}^{t_f} \left( \frac{\partial \hat{y}}{\partial \hat{\boldsymbol{\theta}}} \right)^2 + (\hat{y} - y) \frac{\partial^2 \hat{y}}{\partial \hat{\boldsymbol{\theta}}^2} dt. \quad (22)$$

The first term in (22) is quadratic, i.e.  $\geq 0$ . Under the realistic assumption that the output error  $\hat{y} - y$  is uncorrelated with its derivatives in the components of  $\hat{\boldsymbol{\theta}}$ , the time average of the second term is small. Thus it can be neglected, motivating the Hessian approximation

$$\nabla^2 J(\hat{\boldsymbol{\theta}}) \approx \int_{t_0}^{t_f} \left( \frac{\partial \hat{y}}{\partial \hat{\boldsymbol{\theta}}} \right)^2 dt. \quad (23)$$

## 3. FOTD Model Identification

In this section we utilize the proposed optimization method to obtain FOTD models, parametrized as

$$\hat{P}(s) = \frac{\hat{b}}{s + \hat{a}} e^{-\hat{L}s}, \quad (24)$$

i.e. corresponding to parameter vector  $\hat{\boldsymbol{\theta}} = [\hat{b} \ \hat{a} \ \hat{L}]^T$ . A motivation for choosing a modified relay feedback as the source of input signal is followed by the proposal of a method for finding initial parameters  $\hat{\boldsymbol{\theta}}_0$  for the optimization. Finally, attention is given to some practical implementation related issues.

### 3.1 Input Signal

Existing PID tuning methods such as Ziegler-Nichols [Ziegler and Nichols, 1942],  $\lambda$  [Dahlin, 1968], (A)MIGO [Hägglund and Åström, 2002] as well as a promising MIGO extension, presented by Garpinger [Garpinger and Hägglund, 2008] rely on accurate LF process models. Of particular interest is the phase region  $[-\pi, -\frac{\pi}{2}]$  rad, determining the sensitivity properties of the system. Additionally, the  $\lambda$  and MIGO methods utilize a static gain estimate.

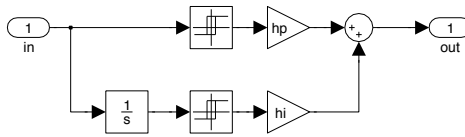


**Figure 1.** Two channel relay.

Describing function analysis indicates that negative feedback connection of a proper, possibly time delayed, monotone LTI system  $P$  and a relay non-linearity results in limit cycle oscillations. The fundamental harmonic of the oscillation occurs at the phase crossover frequency of  $P$ . These observations are the basis of the identification method proposed by Åström and Hägglund in 1984 [Åström and Hägglund, 1984]. Replacing the relay with the two channel (TC) relay non-linearity shown in Fig. 1 allows for an energy concentration at a frequency corresponding to an arbitrary third quadrant phase angle of  $P$ , as described by Friman and Waller in [Friman and Waller, 1997].

The describing function of the TC relay is given by

$$N(a) = \frac{4h_p}{\pi a} - \frac{4h_i}{\pi a}i. \quad (25)$$

The corresponding phase angle is thus

$$\varphi_{TC} = \arctan \left( \frac{h_i}{h_p} \right). \quad (26)$$

By choosing  $h_p, h_i$  the phase of (25) can be chosen arbitrarily in the range  $[0, \frac{\pi}{2}]$  rad, i.e. the fundamental limit cycle will occur at angular frequency  $\omega_\varphi$  corresponding to phase  $\varphi = -\pi + \varphi_{TC} \in [-\pi, -\frac{\pi}{2}]$  rad of  $P$ .

The Fourier series expansion of the symmetric  $T$ -periodic square wave  $u(t)$  with amplitude  $A_u$  is given by

$$u(t) = \sum_{k=1}^{\infty} \frac{4A_u}{\pi k} \sin \left( \frac{2\pi kt}{T} \right). \quad (27)$$

Hence, the input signal energy content at the phase crossover frequency is

$$\frac{\int_T \left( \frac{4A_u}{\pi} \sin \left( \frac{2\pi t}{T} \right) \right)^2 dt}{\int_T u^2(t) dt} = \frac{8}{\pi^2} \approx 0.8, \quad (28)$$

i.e. 80 %, under relay feedback (disregarding the initial convergence phase). Remaining energy lies at integer multiples of the phase crossover frequency.

For the two-channel relay, the above analysis will additionally depend on the LTI system, but the key observations still hold:

- Most input signal energy is issued at the fundamental frequency of the limit cycle oscillation.
- Remaining energy is issued at integer multiples of the fundamental frequency.

If little energy is supplied in the overtones, or if these are heavily attenuated by  $P$ , effectively all identification data originates from the single frequency  $\omega_\varphi$ . Since  $\hat{\theta} = [\hat{b} \ \hat{a} \ \hat{L}]^T$  has three components, this results in an under-determined problem. Generally, if one requires good model fit for a *range* of phase angles, a broader spectrum input is needed. One way to achieve this, is to alter  $\varphi_{TC}$  (by means of  $h_p, h_i$  in (25)) part way through the experiment, and hence obtain frequency data corresponding to at least two separate phase angles  $\varphi_1, \varphi_2$  within the third quadrant. Subsequently, the cost function terms  $J_k$  and its derivatives  $\nabla J, \nabla^2 J$  corresponding to  $\varphi_k$  can be weighted together, with weights  $w_k$  being functions of corresponding signal energies  $E_{y_k}$ , in order to distribute model error over  $\varphi$  in a desired manner.

It is clear, from the above reasoning, that static gain information from obtained models is unreliable. If the aim of identification is to utilize a tuning method explicitly requiring a static gain estimate, e.g.  $\lambda$  or AMIGO, this can be obtained by augmenting the experiment with a step response.

### 3.2 Initial Parameter Values

Since the cost function (2) is non-convex in  $\hat{\theta}$ , a starting point  $\hat{\theta}_0$  close to the global minimum is essential in order to avoid convergence of the Newton-Raphson iteration to a local minimum far from the global one.

Assuming that the process dynamics to be identified are de facto (approximately) FOTD, the following paragraphs suggest a methodology for choosing  $\hat{\boldsymbol{\theta}}_0$ .

The FOTD system (24) can be re-parametrized in normalized time delay  $\hat{\tau} = \frac{\hat{L}}{\hat{L}+1/\hat{a}}$ , average residence time  $\hat{T}_{ar} = 1/\hat{a} + \hat{L}$  and static gain  $\hat{K} = \hat{b}/\hat{a}$ . Of these parameters  $\tau$  is the most difficult to estimate since it requires a separation between delay and lag, while  $\hat{T}_{ar}$  is typically easy to estimate. The following, heuristic, grid-based method aims at yielding a feasible starting point  $\boldsymbol{\theta}_0$  for the Newton-Raphson iteration, by first estimating  $\tau$ .

Assume that the input–output data set  $\{u(t), y(t)\}$ ,  $t \in [t_0, t_f]$  is the outcome of a TC relay feedback experiment. Truncating the data set, only to include the last  $N$  periods of converged limit cycle oscillation yields the new data set  $\{u(t), y(t)\}$ ,  $t \in [t_N, t_f]$ . Let  $A_u$  and  $A_y$  be the amplitudes of the first harmonics in  $u(t)$  and  $y(t)$ ,  $t \in [t_N, t_f]$ , respectively. These are readily given by the Fourier transform as

$$A_u = \left| \frac{2}{t_f - t_N} \int_{t_N}^{t_f} u(t) e^{-i \frac{2\pi N}{t_f - t_N} t} dt \right|, \quad (29)$$

$$A_y = \left| \frac{2}{t_f - t_N} \int_{t_N}^{t_f} y(t) e^{-i \frac{2\pi N}{t_f - t_N} t} dt \right|. \quad (30)$$

The phase- and magnitude of  $\hat{P}(i\omega_\varphi)$ , are given by

$$\angle \hat{P}(i\omega_\varphi) = -\hat{L}\omega_\varphi - \tan^{-1}\left(\frac{1}{\hat{a}}\omega_\varphi\right) = \varphi = -\pi + \varphi_{TC} \quad (31)$$

$$|\hat{P}(i\omega_\varphi)| = A_y \frac{\hat{b}/\hat{a}}{\sqrt{1 + \omega_\varphi^2 (1/\hat{a})^2}} A_u, \quad (32)$$

where  $\varphi_{TC}$  is the TC relay phase from (26). For a given normalized time delay  $\hat{\tau}$  we can insert  $\hat{L} = \frac{\hat{\tau}}{1-\hat{\tau}} \frac{1}{\hat{a}}$  into (31) and solve the resulting convex equation in  $\hat{a}$  numerically. The obtained  $\hat{a}$  can now be inserted into (32), yielding  $\hat{b}$ . By gridding  $\hat{\tau}$ -space we obtain a family of models  $\hat{P}_{\hat{\tau}_i}(s)$ . The cost (2) is evaluated for all  $\hat{P}_{\hat{\tau}_i}(s)$ . Subsequently,  $\hat{\boldsymbol{\theta}}_0$  is chosen to be the parameters of the model corresponding to the smallest cost function value.

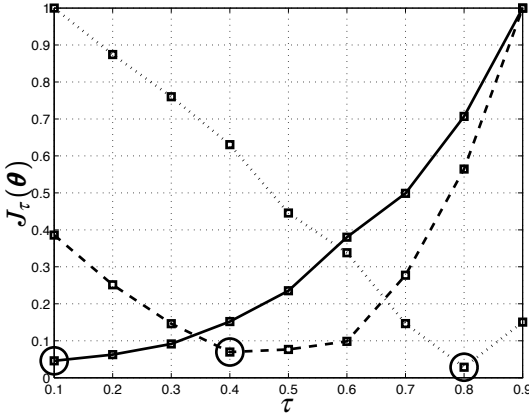


**Figure 2.** Normalized cost  $J_\tau(\theta)/\max J(\theta)$  as function of normalized time delay  $\tau$  for FOTD processes with  $\tau = 0.2$  (solid),  $\tau = 0.5$  (dashed) and  $\tau = 0.8$  (dotted).

The outcome of this procedure is illustrated in Fig. 2 for the FOTD processes  $\theta = [5/4 \ 5/4 \ 1/5]^T \Leftrightarrow \tau = 0.2$  (solid),  $\theta = [2 \ 2 \ 1/2]^T \Leftrightarrow \tau = 0.5$  (dashed) and  $\theta = [5 \ 5 \ 4/5]^T \Leftrightarrow \tau = 0.8$  (dotted), all with average residence time  $T_{ar} = 1.0$  and steady state gain  $K = 1.0$ . Introducing the grid  $\tau_i \in \{0.1i, i = 1..9\}$ , the method yields either the correct  $\tau$  or its grid neighbors.

### 3.3 Model Order Validation

When identifying processes where the order of  $P$  exceeds that of  $\hat{P}$ , an inherent model reduction takes place. The cancellation of one or several poles is compensated for by a change in delay estimate  $\hat{L}$ . If the input  $u$  has a narrow spectrum, the obtained model  $\hat{P}$  can still be accurate around the frequency corresponding to the spectral peak. However, accuracy local to one point might not be enough for feasible controller synthesis.

Therefore, a test for checking the validity of a FOTD model is desirable. An instructive such test is provided in increasing the model order to SOTD and identifying the parameters  $\theta_{0,+}$  of the new model  $\hat{P}_+$ . If

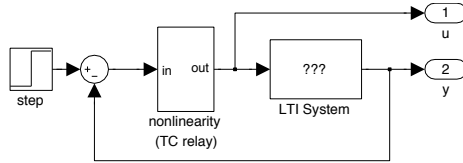


**Figure 3.** Simulink model generating test data for the proposed identification method. The contents of the non-linearity block are shown in Fig. 1. (The step is used to initialize a limit cycle oscillation.)

$|\hat{L} - \hat{L}_+|$  is large compared to  $\hat{L}$ , it is motivated to de facto increase model order to SOTD.

## 4. Experimental Procedure

In this section we outline the experimental procedure. Data was generated in MATLAB/Simulink using the TC relay feedback connection shown in Fig. 3.

### 4.1 Data Generation

Parameters  $h_p, h_i$  in (26) corresponding to  $\varphi_{TC} = 0.4\pi$  rad, i.e.  $\approx 75^\circ$  were chosen. Other  $\varphi_{TC} \in [0, \frac{\pi}{2}]$  rad would shift the phase dependence on model accuracy. However, the identification methodology would remain unaltered.

Each data generating simulation lasted 11 zero crossings of LTI input  $u(t)$ . Identification data was generated for all 133 batch processes.

### 4.2 Identification

In this first paper, we consider the ideal measurement noise and load disturbance free case. The only modifications applied to the above presented theory has been those of discretization (i.e. exchanging integrals for sums, the Fourier transform for the FFT, etc.).

Fundamental frequency amplitudes of in- and outputs were found by applying the FFT versions of (29), (30) on truncated versions of  $u(t), y(t)$ , corresponding to the two last oscillation periods. (As a comment it should be mentioned that the chosen number of relay switches

was found heuristically, so that the last two relay periods could be considered converged limit cycle.)

Subsequently, an initial parameter vector  $\hat{\theta}_0$  was determined by means of (31), (32) and the described  $\hat{\tau}$ -grid method with grid size  $\hat{\tau}_i \in \{0.1i, i = 1..9\}$ .

The Newton-Raphson optimization was applied over 7 iterations, which was found to be adequate, considering cost convergence for the different batch processes.

Back tracking line search, cf. [Boyd and Vandenberghe, 2004], was added to increase convergence rate. The method is illustrated below, with  $\delta$  being the step length, while  $\alpha = 0.25, \beta = 0.5$  are user-defined parameters.

$$\text{while } J(\hat{\theta} + \delta\Delta\hat{\theta}) > J(\hat{\theta}) + \alpha\delta\nabla J(\hat{\theta})^T\Delta\hat{\theta}, \delta := \beta\delta$$

Finally, bounds on time delay estimate  $\hat{L}$  were introduced, forcing it to be strictly non-negative and less than a half period of the fundamental frequency component in  $u(t)$ .

## 5. Results

Results from the identification of one particular transfer function are presented in detail, exploiting key features of the proposed method. This is followed by a compilation of the model errors obtained by running the method on a batch [Åström and Hägglund, 2006].

### 5.1 Instance Study

Here, results from identifying  $P(s) = \frac{1}{(s+1)^2}e^{-s}$  are presented. The choice of process is motivated by the fact that process order is higher than model order. This has two fundamental implications:

- There exists no FOTD model with 'good' fit for all frequencies. However, the proposed method is expected to yield one with good fit around the phase  $\varphi$  in the third quadrant.
- The initial guess provided by  $\hat{\tau}$ -gridding is sub-optimal, since the model structure assumption is invalid, demonstrating the benefit of the Newton-Raphson optimization.

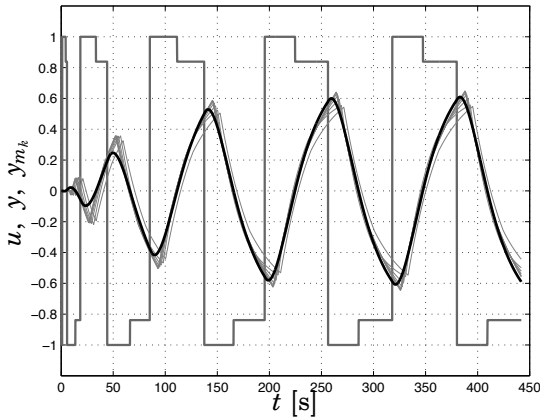


**Figure 4.** TC relay output  $u(t)$  (grey), process output  $y(t)$  (solid, black) and converging model outputs  $y_{m_k}(t)$ ,  $k \in \{1, \dots, 7\}$  (grey, thin).

Fig. 4 shows identification input  $u(t)$ , generated by the TC relay feedback, together with corresponding process output and converging model output.

Fig. 5 shows the Nyquist curve of  $P$  together with those of the obtained FOTD model  $\hat{P}$  and the corresponding initial model  $\hat{P}_0$  provided by the  $\tau$ -gridding. Not unexpectedly,  $\hat{P}_0$  provides a better all-over fit, whereas  $\hat{P}$  shows a better fit in the third quadrant (which is achieved at expense of a worse fourth quadrant fit). Both models provide good fits at the phase angle  $\varphi = -\pi + \varphi_{TC}$ , corresponding to the fundamental harmonic of the process input  $u(t)$ .

The observations presented above generally hold for the AMIGO batch.

A complementary representation of performance is given by the step response. Fig. 6 shows the step responses of  $P$ ,  $\hat{P}$  and  $\hat{P}_0$  in Fig. 5.

As expected, the final model  $\hat{P}$  has a worse static gain estimate than the initial model  $\hat{P}_0$ .

Note the over-estimation of  $L$ , shown in the lower plot of Fig. 6, being a consequence of lower model than process order. A second order

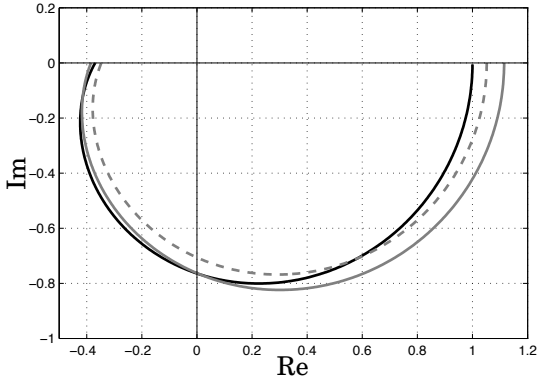


**Figure 5.** Nyquist curve of  $P(s) = \frac{1}{(s+1)^2}e^{-s}$  (black),  $\hat{P}_0(s) = \frac{0.52}{s+0.49}e^{-1.35s}$  (grey, dashed) and  $\hat{P}(s) = \frac{0.57}{s+0.51}e^{-1.37s}$  (grey, solid).

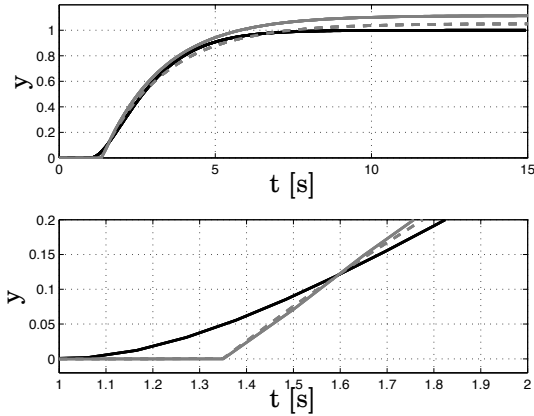


**Figure 6.** Step response of  $P(s) = \frac{1}{(s+1)^2}e^{-s}$  (black),  $\hat{P}_0(s) = \frac{0.52}{s+0.49}e^{-1.35s}$  (grey, dashed) and  $\hat{P}(s) = \frac{0.57}{s+0.51}e^{-1.37s}$  (grey, solid). The lower plot is a magnification of the bottom left part of the upper plot.

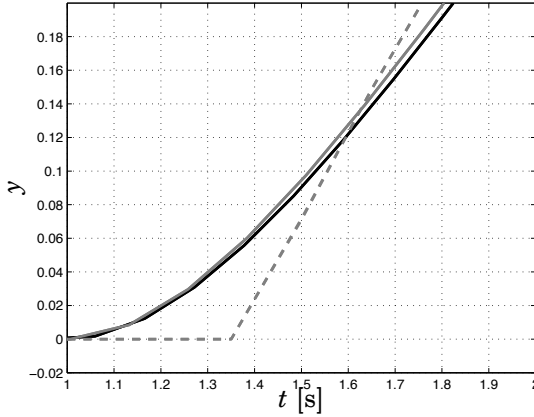


**Figure 7.** Step responses of  $P(s) = \frac{1}{(s+1)^2}e^{-s}$ ,  $\hat{P}(s) = \frac{0.57}{s+0.51}e^{-1.37s}$  and  $\hat{P}_+(s) = \frac{0.001s+1.06}{(s+1.26)(s+0.84)}e^{-1.01s}$

model (provided a feasible  $\theta_{+,0}$  is given by

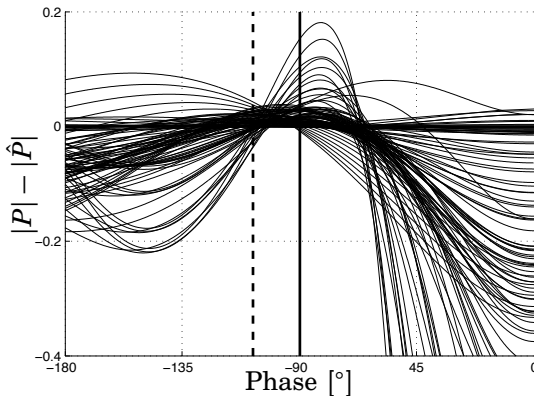
$$\hat{P}_+(s) = \frac{0.001s + 1.06}{(s + 1.26)(s + 0.84)}e^{-1.01s}. \quad (33)$$

Fig. 7 shows the initial part of the step responses of  $P$ ,  $\hat{P}$  and  $\hat{P}_+$ .

The model order test of section 3 yields

$$\frac{|\hat{L} - \hat{L}_+|}{\hat{L}} = 0.26. \quad (34)$$

Another interesting observation is that  $\hat{T}_{ar} = 3.33$  for the FOTD model and  $\hat{T}_{+,ar} = 2.98$  for the SOTD model, which are both good estimates, given  $T_{ar} = 3.0$  for the process. However, assume all input energy was issued at the frequency  $\omega_\varphi$ , i.e.  $u(t) = \sin(\omega_\varphi t)$ . Asymptotically the cost would be minimized (to  $J = 0$ ) when  $|P(i\omega_\varphi)| = |\hat{P}(i\omega_\varphi)|$  and  $\angle P(i\omega_\varphi) = \angle \hat{P}(i\omega_\varphi)$ , where the left hand sides are constants and the right hand sides are given by (32) and (31), respectively. This is an under-determined system in  $\hat{\theta}$ , with unique solution  $\forall \hat{L} \in \mathbb{R}_+$ , as indicated in section 3.



**Figure 8.** Gain error  $|P| - |\hat{P}|$  as function of process phase for the processes of the AMIGO test batch.

## 5.2 Batch Study

Fig. 8 shows a compilation of gain errors  $|P| - |\hat{P}|$  plotted against process phase, for the processes of the test batch.

As expected, the method yields best fit close to the phase  $-115^\circ$  corresponding to the first harmonic of the input signal  $u(t)$  (marked by a dashed line in Fig. 8).

For larger negative phase values within the third quadrant, the errors are negative for most processes, corresponding to conservative models, concerning sensitivity.

## 6. Conclusions

A method for computing partial derivatives of the output error in model transfer function parameters has served as basis for a gradient search (Newton-Raphson) approach to system identification. The method is applicable to all proper, possibly time delayed, transfer functions.

The following, highly interrelated, items need to be decided, prior to applying the method: cost function, model order (choice and verifica-

tion), input signal, initial parameters and halting criterion. Particular attention has to be given to the input signal, ensuring spectral content at frequencies for which model validity is crucial.

This paper was mainly confined to the case of FOTD model structure, utilizing a quadratic cost function and TC relay feedback for input generation.

Initial parameters were obtained by means of a heuristic gridding strategy and no explicit attention was given to halting criteria for the optimization.

A method for model order validation was suggested.

The approach proved successful for a large number of common process types and instances thereof.

## 7. Future Work

There are several directions for potential future work related to the proposed identification method.

One obvious continuation would be to combine the identification method with one or several PID-tuning methods and evaluate the obtained closed loop performance. A related issue is the investigation of how process- and measurement noise affect the identification and ultimately the closed loop performance.

Another interesting direction is that of MIMO control. Especially TITO systems are common in process industry. Hence an extension of the method to the identification of TITO dynamics would be of high interest.

It would also be interesting to evaluate performance of the method using higher order models, possibly with modifications regarding cost function and input signal. SOTD models (with one zero) are of particular interest, covering essentially all modeling needs for PID design.

## References

- Åström, K. J. and T. Bohlin (1965): “Numerical identification of linear dynamic systems from normal operating records.” In *Proc. IFAC Conference on Self-Adaptive Control Systems*. Teddington, UK.
- Åström, K. J. and T. Häggglund (1984): “Automatic tuning of simple regulators with specifications on phase and amplitude margins.” *Automatica*, **20**, pp. 645–651.
- Åström, K. J. and T. Häggglund (2006): *Advanced PID Control*. ISA.
- Boyd, S. and L. Vandenberghe (2004): *Convex Optimization*. Cambridge.
- Dahlin, E. B. (1968): “Designing and tuning digital controllers.” *Instruments and Control Systems*, **42**, June, pp. 77–83.
- Friman, M. and K. V. Waller (1997): “A two-channel relay for autotuning.” *Industrial and Engineering Chemistry Research*, **36**, pp. 2662–2671.
- Garpinger, O. and T. Häggglund (2008): “A software tool for robust PID design.” In *Proc. 17th IFAC World Congress, Seoul, Korea*.
- Häggglund, T. and K. J. Åström (2002): “Revisiting the Ziegler-Nichols tuning rules for PI control.” *Asian Journal of Control*, **4:4**, pp. 364–380.
- Lilja, M. (1988): “Least squares fitting to a rational transfer function with time delay.” In *Preprints Control '88*. IEEE, Oxford.
- Lilja, M. (1989): *Controller Design by Frequency Domain Approximation*. PhD thesis TFRT-1031, Department of Automatic Control, Lund University, Sweden.
- Ziegler, J. G. and N. B. Nichols (1942): “Optimum settings for automatic controllers.” *Transaction fo the ASME*, pp. 759–768.

# Paper III

## **Individualized PID Control of Depth of Anesthesia Based on Patient Model Identification During the Induction Phase of Anesthesia**

**Kristian Soltesz   Jin-Oh Hahn   Guy A. Dumont  
J. Mark Ansermino**

### **Abstract**

This paper proposes a closed-loop propofol admission strategy for depth of hypnosis control in anesthesia. A population-based, robustly tuned controller brings the patient to a desired level of hypnosis. The novelty lies in individualizing the controller once a stable level of hypnosis is reached. This is based on the identified patient parameters and enhances suppression of output disturbances, representing surgical stimuli. The system was evaluated in simulation on models of 44 patients obtained from clinical trials. A large amount of improvement (20 – 30%) in load suppression performance is obtained by the proposed individualized control.

©2011 IEEE CDC/ECC. Reprinted, with permission, from *Proceedings of the 2011 IEEE Conference on Decision and Control and European Control Conference*. Orlando, USA, 2011. The article has been modified to fit the current format. Discovered typographical errors have been corrected in this reprint.

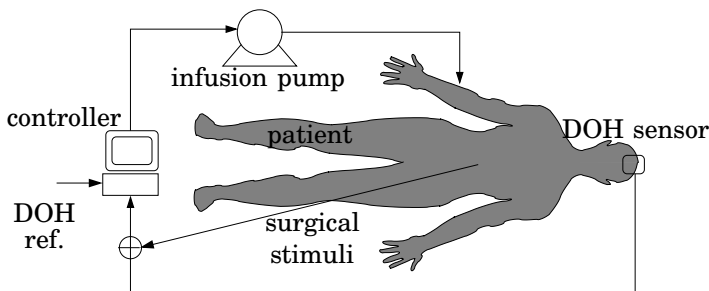


**Figure 1.** Closed-loop DOH control system.

## 1. Introduction

During surgical procedures, a combination of anesthetic drugs are given in order to 1) maintain a desired depth of hypnosis (sleep), 2) keep the patient in an analgesic (pain free) state, and in some cases 3) establish a neuro-muscular blockade to avoid movement. This paper focuses on the problem of individualized closed-loop control of depth of hypnosis (DOH) based on propofol administration. Fig. 1 outlines the system from a control engineering point of view.

Propofol hypnosis can be divided into three temporal phases. During the *induction* phase, the aim is to bring the patient to a reference DOH level. Once a stable DOH close to the reference is achieved, the *maintenance* phase, during which surgery takes place, begins. The surgical stimuli can be viewed as output disturbances, reducing the DOH. At the same time, the administration of analgesic drugs increase the DOH via anesthetic-opioid synergy. Hence, the challenge during the maintenance phase is to administer propofol to counteract the disturbances, without over- or under-dosing. Once surgery is completed, the *emergence* phase, during which administration of propofol is terminated, takes place.

The aim of this paper is to examine the potential benefit of individualized propofol delivery based on controller re-tuning at the end of the induction phase. The main advantage of a single update before the maintenance phase begins, as opposed to continuous adaptation (see e.g. [Haddad *et al.*, 2006]), is that unmeasured disturbances dur-

ing the maintenance phase do not result in poor performance or even instability due to drifting parameters. Focus does not lie on the controller tuning per se, but rather on what can be gained by the proposed individualization. The rationale supporting this paper can therefore be combined with previous work in the area of closed-loop propofol anesthesia, such as [Gentilini *et al.*, 2001], [Ionescu *et al.*, 2008] and [Dumont *et al.*, 2009].

The paper is organized as follows: Section 2 presents the models that controller synthesis is based upon. The PID controller and its tuning is explained in Section 3. Patient model parameter identification for individualized control is the topic of Section 4. The proposed control scheme is evaluated in a simulator, explained in Section 5. Simulation results are presented and discussed in Section 6. Finally, conclusions are drawn in Section 7.

## 2. Model of the Propofol-DOH Process

Patient models for anesthesia consist of a pharmacokinetic (PK) model explaining the distribution and metabolism of the drug, and a pharmacodynamic model relating the plasma drug concentration to clinician effect. In a previous work [Bibian *et al.*, 2005] PK and PD parameters were derived from demographic data, based on which robust controllers were synthesized to handle inter- and intra-patient variability.

Controller and PD identifier were designed based on the patient PKPD model with the propofol infusion rate  $u$  as input and the DOH measurement  $y$  as output.

### 2.1 Parameters and Signals

Table 1 lists signals and parameters used throughout the paper.

**Table 1.** Signals and parameters.

Symbol	Unit/Range	Name
<b>A, B, C</b>	-	Schüttler PK system matrices
$C_e$	mg.l <sup>-1</sup>	Effect site concentration
$C_p$	mg.l <sup>-1</sup>	Primary compartment concentration
$C_{p_m}$	mg.l <sup>-1</sup>	Estimate of $C_p$ from $E_m$
DOH	(100,0)	Depth of hypnosis (100 ⇔ awake)
$e_L$	-	Load step control error
$E$	(0,1)	Normalized DOH (0 ⇔ awake)
$E_m$	(0,1)	Estimate of $E$ from $y$
$E_{m\sigma}$	-	Signal threshold
$EC_{50}$	mg.l <sup>-1</sup>	Hill gain parameter
$h$	s	Controller sample period
$k_{ij}, j = 1, 2, 3$	s <sup>-1</sup>	Rate constants (flow $i \rightarrow j$ )
$k_d^{-1}$	s	Effect PD time constant
$k_{10}$	s <sup>-1</sup>	Elimination rate constant
$K$	-	True FOTD gain
$\hat{K}$	-	Estimate of $K$
$K_D$	-	Derivative controller gain
$K_I$	-	Integral controller gain
$K_P$	-	Proportional controller gain
$L$	-	True FOTD delay
$\hat{L}$	-	Estimate of $L$
$N$	-	Maximal derivative gain
$p_k, k = 1, 2, 3$	-	Schüttler PK poles
$r$	(0,1)	Normalized DOH reference
$t_\gamma$	s	Duration of $\gamma$ identification
$t_{ind}$	s	Duration of induction phase

Continued on next page

**Table 1.** – Continued from previous page.

Symbol	Unit/Range	Name
$T$	-	True FOTD time constant
$\hat{T}$	-	Estimate of $T$
$T_d$	s	Effect PD delay
$T_I$	s	Controller integral time
$T_D$	s	Controller derivative time
$T_r$	s	Reference filter time constant
$T_t$	s	Anti-windup tracking time
$u$	mg·s <sup>-1</sup>	Infusion rate
$u_{\max}$	mg·s <sup>-1</sup>	Upper bound of control signal
$u_{\min}$	mg·s <sup>-1</sup>	Lower bound of control signal
$u_\sigma$	-	Signal threshold
$v$	-	Signal in Hill function
$\hat{v}$	-	Feedback quantity
$v_m$	-	Estimate of $v$ from $E$
$V_1$	l	Primary compartment volume
$\mathbf{x} = [x_1 \ x_2 \ x_3]^T$	mg·l <sup>-1</sup>	Compartment concentrations
$x_D$	-	PID derivative filter state
$x_I$	-	PID integrator state
$y$	(0,1)	Normalized measured DOH
$\gamma$	-	Hill slope parameter
$\hat{\gamma}$	-	Estimate of $\gamma$

## 2.2 Pharmacokinetic (PK) Model

The PK model relates infusion rate  $u$  to plasma concentration  $C_p$ . In this paper, the Schüttler PK model [Schüttler and Ihmsen, 2000] was used. It is a three-compartment mamillary model, outlined in Fig. 2. Each compartment represents a class of tissues. The drug is delivered

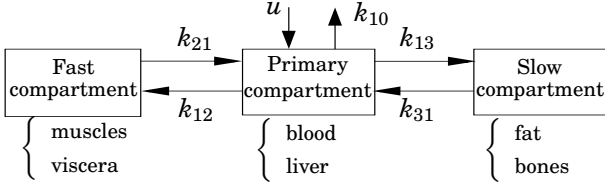


**Figure 2.** Schüttler’s three-compartment mammillary model.

into the primary (central) compartment with rate  $u$ . Denoting by  $\mathbf{x}$  the vector of drug concentration in each compartment, the Schüttler’s model is given by

$$\dot{\mathbf{x}} = \begin{bmatrix} -(k_{10} + k_{12} + k_{13}) & k_{12} & k_{13} \\ k_{21} & -k_{21} & 0 \\ k_{31} & 0 & -k_{31} \end{bmatrix} \mathbf{x} + \frac{1}{V_1} \begin{bmatrix} 1 \\ 0 \\ 0 \end{bmatrix} u. \quad (1)$$

The transfer function representation of (1) from  $u$  to  $x_1$  is

$$G_{C_p, u}(s) = \frac{1}{V_1} \frac{(s + k_{21})(s + k_{31})}{(s + p_1)(s + p_2)(s + p_3)}, \quad (2)$$

where  $p_k$ ,  $k \in \{1, 2, 3\}$  are defined accordingly from  $k_{ij}$ . It was concluded by Schüttler et al. [Schüttler and Ihmsen, 2000] that *age* and *lean body mass* are reliable demographic covariates for the parameters of (2). Functions relating these covariates to volumes and clearance rates  $V_1, k_k$ ,  $k \in \{1, 2, 3\}$  are presented in [Schüttler and Ihmsen, 2000].

### 2.3 Pharmacodynamic (PD) Model – Hill Function

**Effect Site Dynamics** The output of the Schüttler PK model is the primary compartment concentration of propofol,  $C_p$ . However, the effect site of the drug is the brain, not the plasma. To account for the distribution of drug from the plasma to the effect site, the PK model was augmented by a delayed first order system [Bibian, 2006]:

$$G_{C_e, C_p}(s) = \frac{k_d}{s + k_d} e^{-T_d s}, \quad (3)$$

where the delay is intended to model the drug transport from the intravenous to the effect site.

**Dose-Response Characteristics** The clinical effect  $E$  is normalized to  $(0, 1)$ , where 0 corresponds to fully awake state. In the steady state, the relation between  $C_e$  and  $E$  is well described by a sigmoidal  $E_{\max}$  function:

$$E(C_e) = \frac{C_e^\gamma}{EC_{50}^\gamma + C_e^\gamma}, \quad (4)$$

which is also known as the Hill function. It is parametrized by  $EC_{50}$ , the value of  $C_e$  corresponding to  $E = 0.5$ , and  $\gamma$ , defining the steepness of the sigmoidal curve. The Hill function (4) can be decomposed into a series of a linear gain

$$v(C_e) = \frac{1}{2EC_{50}} C_e, \quad (5)$$

and a sigmoidal nonlinearity

$$E = f(v; \gamma) = \frac{v^\gamma}{\frac{1}{2} + v^\gamma}, \quad (6)$$

which is parametrized only in  $\gamma$ . It is obvious from (6) that  $E = 0.5$  corresponds to  $v = 0.5$ .

For model identification purposes, the effect PD and linear Hill gain are lumped together to yield the following first order time delayed (FOTD) system:

$$v(s) = \frac{K_d/(2EC_{50})}{s + K_d} e^{-sT_d} C_p(s), \quad (7)$$

whereas the nonlinear part (6) is treated separately.

## 2.4 Clinical Front End

There are several clinical options for measuring DOH based on the electroencephalogram (EEG), which can be sampled using non-invasive probes mounted on the patient's forehead. The most popular option is the Bispectral Index (BIS) [Johansen and Sebel, 2000], for which

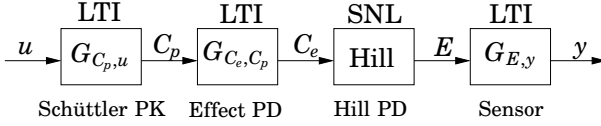


**Figure 3.** PKPD patient and sensor model, relating DOH  $y$  to propofol infusion rate  $u$ . Subsystems are linear time invariant (LTI) or static nonlinearities (SNL).

commercial instrumentation equipment are available. However, BIS is not ideal for control design purposes since its dynamics are strongly time-varying and that the proprietary algorithm often exhibits non-linear behavior. The use of wavelet techniques has been proposed to overcome these challenges, yielding the  $WAV_{CNS}$  index [Zikov *et al.*, 2006]. It correlates well with BIS, and moreover, it has time-invariant linear dynamics:

$$G_{y,E}(s) = \frac{1}{(8s + 1)^2}, \quad (8)$$

which is preferable to BIS from a control design perspective. The  $WAV_{CNS}$  monitor is graded in BIS units. They range  $(0, 100)$ , where 100 corresponds to the fully awake state.

## 2.5 PKPD Model

The patient model is obtained by combining the PK and PD models. A block diagram of this combination, together with the  $WAV_{CNS}$  monitor, is shown in Fig. 3.

It was demonstrated that PK parameters of propofol are linear in the range  $25 - 200 \mu\text{g}\cdot\text{kg}^{-1}\cdot\text{min}^{-1}$  and that the model is generally invalid outside this range [Schnider *et al.*, 1998b]. Similarly, the Hill function (4) describes the steady-state relation between  $C_e$  and  $E$ .

## 2.6 Surgical Stimuli

Surgical stimulation was modeled as an output disturbance, which was adapted from [Dumont *et al.*, 2009] (see Fig. 4).

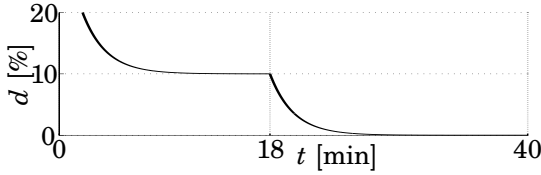


**Figure 4.** Disturbance profile from [Dumont *et al.*, 2009].

### 3. Robust PID Control Synthesis

A two-degrees-of-freedom PID controller was designed for DOH control. Two novel output filters were introduced in this paper in an effort to facilitate control design by effectively cancelling out the monitor dynamics and the Hill function nonlinearity.

#### 3.1 Output Filter I

The system shown in Fig. 3 cannot be readily divided into its LTI and static nonlinearity components, due to the existence of the Hill function between the effect PD and the monitor dynamics. This is a limiting factor in both patient model identification and controller synthesis. To overcome this problem, we propose to augment a delayed inverse of the monitor dynamics as follows. The control system operates at 1 Hz. A zero order hold (ZOH) sampling of (8) with period  $h = 1$  s yields

$$G_{y,E}^h(z) = \frac{1}{100} \frac{0.719z + 0.662}{z^2 - 1.765z + 0.778}. \quad (9)$$

To invert (9) without introducing acausality, a delay of  $h$  was added, resulting in the delayed inverse:

$$F_1(z) = 100 \frac{z^2 - 1.765z + 0.778}{0.719z^2 + 0.662z}. \quad (10)$$

This filter was applied to the sensor output to convert the system dynamics to a standard Wiener model by canceling out the effect of the monitor dynamics. The sensor plus the delayed inverse was modeled as a delay  $h$  in controller synthesis. Depending on the high pass nature of the drug delivery actuator, further filtering might therefore be desirable.

### 3.2 Output Filter II

The model in Fig. 3 is nonlinear due to the Hill function. In the context of synthesizing a maintenance phase controller, this can be approached by linearizing (4) around the operating point  $C_e = EC_{50}$ . However, this is not acceptable during the induction phase, in which no well-defined operating point exists. If a PID controller (or any controller involving integral action) is used, the integral state will build up rapidly during the beginning of the induction phase due to the low dose concentrations,  $C_p \ll EC_{50}$ . This will in turn cause an undershoot of the  $WAV_{CNS}$  response. A possible remedy to alleviate this problem is to reduce the integral action, but this may increase the duration of the induction phase. To facilitate the controller design by further linearizing the system dynamics, an additional linearizing filter was used in series with (10) as follows. The inverse of the non-linear part of the Hill function (6) is given by

$$v = F_2(E; \gamma) = f^{-1}(E; \gamma) = \frac{1}{2} \left( \frac{E}{1-E} \right)^{\frac{1}{\gamma}}. \quad (11)$$

Letting  $\gamma$  and  $\hat{\gamma}$  be the true and demographics-based slope parameters, respectively, yields

$$\hat{v} = f^{-1}(f(v; \gamma); \hat{\gamma}) = \frac{1}{2}(2v)^{\gamma/\hat{\gamma}}, \quad (12)$$

which is close to  $v$  when  $\hat{\gamma} \approx \gamma$ . The controller was based on the assumption that  $\hat{\gamma} = \gamma$  and that the nonlinearity was completely cancelled out by closing the loop from  $\hat{v}$  in (12).

### 3.3 Plant Model

Combining (2), (3), (5), (9), (10) and (12) and assuming  $\hat{\gamma} = \gamma$  yields the plant model

$$P(s) = \frac{k_d}{2EC_{50}V_1} \frac{(s + k_{21})(s + k_{31})e^{-s(T_d+h)}}{(s + p_1)(s + p_2)(s + p_3)(s + k_d)}, \quad (13)$$

which was used for controller synthesis.

### 3.4 Controller

The PID controller was parametrized in its proportional ( $K_p$ ), integral ( $K_I$ ) and derivative ( $K_D$ ) gains. Two robust PID design methods, outlined below, were evaluated to determine these gains. They are both based on minimizing norms of the tracking error caused by step load disturbances.

**Robust Load IE Minimization** The objective of this method is to find PID parameters  $\{K_P, K_I, K_D\}$  that minimize the integral of the control error (IE)  $e_L$  caused by a step load disturbance. Robustness is enforced by restricting the open-loop Nyquist curve outside a circular disc with radius  $M_s$ , centered at  $-1$ . This is equivalent to restricting the  $\infty$ -norm of the sensitivity function:

$$\min_{K_P, K_I, K_D} \int_0^{\infty} e_L(\tau) d\tau, \quad (14)$$

$$s.t. \max_{\omega} |S(\omega)| \leq M_s. \quad (15)$$

See [Panagopoulos *et al.*, 2002] for a thorough description of the method or [Åström and Hägglund, 2006] for a summary. A regimen for determining suitable  $M_s$  is described in [Dumont *et al.*, 2009].

**Robust Load IAE Minimization** An oscillatory zero-mean error can yield small IE values, yet is not desirable. This can be prevented by using the following optimization constraint:

$$\min_{K_P, K_I, K_D} \int_0^{\infty} |e_L(\tau)| d\tau. \quad (16)$$

The minimized quantity is referred to as the integral absolute error (IAE). A useful algorithm is presented in [Garpinger and Hägglund, 2008].

### 3.5 Reference Filter

In order to avoid oscillations and over-dosing during the induction phase, the reference was processed using the following filter, whose time constant  $T_r$  was chosen according to [Martinez, 2005].

$$F_r(s) = \frac{1}{sT_r + 1}. \quad (17)$$

### 3.6 Implementation Aspects

**Saturation and Integrator Anti-Windup** The control signal has a natural lower bound  $u_{\min} = 0$  (since drug cannot be extracted once infused). For safety reasons, an upper bound  $u_{\max}$  of  $3.33 \text{ mg}\cdot\text{s}^{-1}$  was also introduced. Tracking was utilized in order to avoid integral windup; see Fig. 2.5(b). The tracking constant was heuristically chosen as the geometric mean of the PID integral ( $T_I = \frac{K_P}{K_I}$ ) and derivative ( $T_D = \frac{K_D}{K_P}$ ) times as suggested in [Åström and Hägglund, 2006]:

$$T_t = \sqrt{T_I T_D} = \sqrt{\frac{K_D}{K_I}}. \quad (18)$$

**Setpoint Weighting** In this paper, disturbance rejection and absence of output oscillations are prioritized to tight reference tracking. Hence, a zero setpoint weight was chosen for proportional and derivative components of the controller, forcing the reference to enter the control signal only through the integral term, as shown in Fig. 2.5(b).

**Derivative Filter** To suppress the high frequency noise, the differentiator  $K_D s$  was filtered as

$$\frac{s K_P K_D N}{s K_D + K_P N}, \quad (19)$$

where  $N = 5$  was chosen heuristically to yield an adequate trade off between noise suppression and phase lead. Note that the reference was not differentiated to facilitate a smooth response to rapid and abrupt reference changes.

**Derivative Kick** The low-pass reference filter combined with the zero setpoint weight resulted in a slow increase of  $u$ , and consequently  $y$ , during the beginning of the induction phase, which is not desirable, since the propofol infusion is painful to the patient while the DOH is low. To avoid this problem, the derivative term of the PID control signal was set to a strictly positive value during the beginning of the induction phase, yielding a spike in  $u$ .

**Discretization** The controller was discretized using the approximation  $s \approx z - 1$ , which is acceptable since the sample period is small compared to the dominant time scale of the system. Using ZOH discretization or performing the tuning optimization in the discrete time domain would have been other options. However, they lack the intuitive insight provided by the continuous-time PID control architecture that the proposed discretization preserves.

**Bumpless Parameter Changes** Let  $x_I$  and  $x_D$  be the state of the PID integrator and derivative filter, shown in Fig. 2.5(b) and Fig. 2.5(c). The control signal is given by

$$u = \text{sat}_{u_{\min}}^{u_{\max}} \left( \underbrace{-\hat{v}K_P}_P + \underbrace{x_I}_I \underbrace{-\hat{v}K_P N - x_D \frac{K_P N}{K_D}}_D \right). \quad (20)$$

Switching the set of PID controller parameters from  $\{K_P, K_I, K_D\}$  to  $\{K'_P, K'_I, K'_D\}$  at the end of the induction phase, may lead to discontinuity in the derivative term, resulting in discontinuity in the control signal. This risk was prevented by simultaneously updating the states as follows:

$$x'_D = \hat{v}(K'_D - K_P) \frac{K'_D}{K'_P} - x_D \frac{K_P}{K_D} \frac{K'_D}{K'_P}, \quad (21)$$

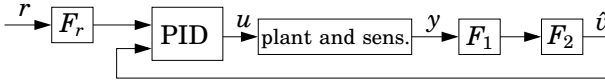
$$x'_I = x_I + \hat{v}(K'_P - K_P). \quad (22)$$

### 3.7 Closed-Loop System

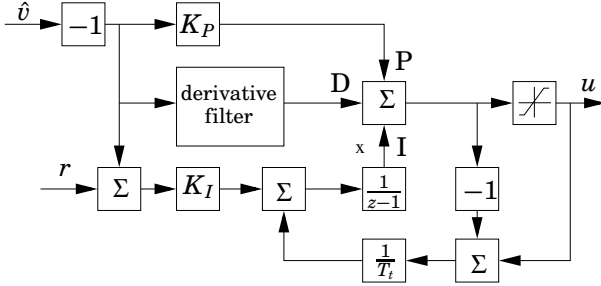
Summarizing, Fig. 2.5(a) shows the block diagram of the closed loop system, including patient, controller and filters, discussed above. The block diagram of the PID controller is shown in Fig. 2.5(b). The derivative filter block of Fig. 2.5(b) is illustrated in detail in Fig. 2.5(c).

## 4. System Identification

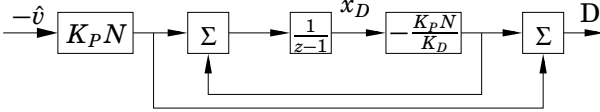
The objective of the system identification was to derive parameter estimates for the model that relates  $C_p$  to  $E$ ; see Fig. 3. The model consists



(a) Closed-loop system. The plant and sensor is equivalent to Fig. 3.



(b) PID controller. The derivative filter block contains the ZOH discretization of (19).



(c) The derivative filter (19) block of Fig. 2.5(b).

**Figure 5.** Closed-loop system and PID controller.

of the FOTD (7), parametrized in

$$K = \frac{1}{2EC_{50}}, \quad T = \frac{1}{K_d}, \quad L = T_d, \quad (23)$$

and the nonlinear part of the Hill function (6), parametrized in  $\gamma$ . Since  $E$  is not directly available, its estimate  $E_m$  was used. It was obtained by applying  $F_1$  in (10) to  $y$ . Likewise, an estimate  $C_{p_m}$  of  $C_p$ , obtained by driving the PK model (2) with  $u$ , was used.

### 4.1 Hill Function Nonlinearity

Since  $v$  in (7) ranges from 0 to  $\approx 0.5$  during the induction phase, linearizing (7) around a nominal value does not present a feasible approach towards PD model parameter identification. Furthermore, it is not trivial to simultaneously identify the LTI parameters  $\{K, T, L\}$  and the Hill function parameter  $\gamma$ . For this reason a two-stage approach was employed. The parameter  $\gamma$  was identified and fixed during the first stage and LTI parameters were identified during the second stage.

### 4.2 Initial Parameter Estimates

Inspecting the simulation pairs of  $u$  and  $E$  reveals that the first order dynamics are fast compared with the time scale of induction. Hence, it was reasonable to approximate (7) by a delayed gain  $K \cdot e^{-Ls}$ .

The initial estimate  $\hat{L}$  of  $L$  was obtained by identifying the time instants after which  $E_m$  and  $u$  stay above thresholds  $E_{m\sigma}$  and  $u_\sigma$ , respectively. The initial estimate  $\hat{K}$  of  $K$  was then obtained by averaging the ratio of  $E_m$  and  $u$  over the last 3 min of the induction phase.

Subsequently, the initial estimate  $\hat{\gamma}$  of  $\gamma$  was obtained by a bisection search, which minimized (the discretized equivalent of)

$$\int_0^{t_y} (f^{-1}(E_m; \hat{\gamma})(t) - KC_{p_m}(t + L))^2 dt. \quad (24)$$

Fixing  $\hat{\gamma}$  yielded the estimate  $v_m$  of  $v$ :

$$v_m = f^{-1}(E_m; \hat{\gamma}). \quad (25)$$

Finally, a bisection search was used to find the estimate  $\hat{T}$  of  $T$ , which minimized (the discretized equivalent of)

$$\int_0^{t_{\text{ind}}} \left( v_m(t) - \mathcal{L}^{-1} \left( \frac{\hat{K} e^{-s\hat{L}}}{s\hat{T} + 1} C_{p_m} \right) \right)^2 dt. \quad (26)$$

### 4.3 PD Identification Using Induction Phase Response

A gradient-based identification method [Soltesz *et al.*, 2010] was employed to obtain refined estimates of the PD model parameters from

the patient’s response during the induction phase. The parameter estimates were identified to minimize

$$J(\hat{\theta}) = \int_0^{t_{\text{ind}}} (v_m - \hat{v})^2 dt, \quad (27)$$

where  $v_m$  was parametrized in  $\hat{\theta} = \{K, T, L\}$  (while  $\hat{\gamma}$  was fixed). Computing the gradient  $\nabla J(\hat{\theta})$  was done by simulating an augmented system, where the augmented states were partial derivatives of the objective function (27) with respect to the PD model parameters to be identified. Details of the methods are outlined in [Soltesz *et al.*, 2010].

## 5. Simulated Experiment

The surgical procedure was simulated for each patient in the test population, as described below.

### 5.1 Test Population

The test population consisted of 44 PKPD models. Model parameters were derived using clinical data and are disclosed in [Dumont *et al.*, 2009]. In the course of PD identification, it was assumed that individual PK models can be accurately characterized using Schüttler’s covariate formulae [Schüttler and Ihmsen, 2000]. This essentially lumps all the parametric uncertainty into the PD model.

### 5.2 Experiment Layout

***Induction Phase*** Prior to the simulated surgical procedure, the induction phase controller was synthesized according to Section 3, based on the control design model (13). Parameters  $k_{21}, k_{31}, p_1, p_2$  and  $p_3$  were computed from the patient age and weight using Schüttler’s formulae, while population averages were used for  $K_d, EC_{50}$  and  $T_d$ . Propofol was administered using this population-based controller during the induction phase of the simulated surgical procedure.

***PD Identification and Controller Re-Design*** PD parameters were estimated as described in Section 4. At the end of the induction phase, the estimated PD parameters were used to synthesize an individualized controller, based on the same procedure as the induction phase controller.

***Maintenance and Emergence Phases*** During the beginning of the maintenance phase, the simulation state was saved to allow for parallel maintenance phase simulations with (i) the induction phase controller, (ii) the individualized controller and (iii) an ideal controller based on the actual parameter values of the simulated patient. Signals from these simulations were saved and analyzed as described in Section 6.

### 5.3 PK Uncertainty

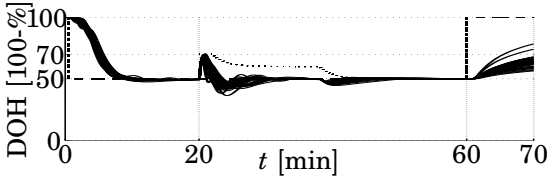
In order to introduce a realistic amount of PK uncertainty in the simulated procedure, perturbations were given to the parameters of the patient model. This was done using normally distributed random numbers with standard deviations chosen as the standard deviations of the prediction residuals reported in Schüttler et al. [Schüttler and Ihmsen, 2000]. Nominal values were used for the controller synthesis.

## 6. Results and Discussion

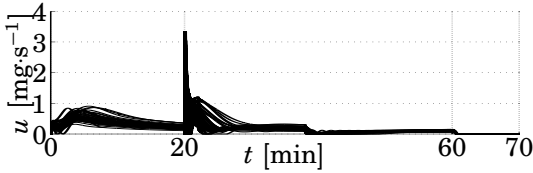
Overall, the individualized controller outperformed the population-based controller. Fig. 6 shows the simulation profiles for each of the 44 patients, using the individualized controller. In terms of IAE, the individualized controller could provide a 23 % reduction in error over the 44 patient models, compared with the population-based controller. Moreover, it was only 4 % larger than with the ideal controller, synthesized using the true patient PKPD models. The results clearly demonstrate the potential of an individualized control scheme.

The use of an output filter (11) significantly improved the reference tracking performance in the induction phase. In the absence of the filter, undershoots by as much as 30 BIS units were observed in some patients.

Due to the presence of the perturbations in the PK models, the identified PD parameters generally did not converge to the patient values.



(a) Measured DOH with disturbance profile of Fig. 4.



(b) Infusion profiles with disturbance profile of Fig. 4.

**Figure 6.** Measured DOH and infusion profiles of the test population.

Instead they converged to values close to their true counterparts in order to compensate for the PK mismatch. It should be noted, however, that the identified PD parameters converged to the true parameter values when the PK model uncertainty was not considered.

Although rigorous parameter convergence proof is not feasible due to the non-convexity of the system identification problem discussed in Section 4, the proposed two-stage identification strategy was able to provide accurate parameter estimates for all the simulated procedures. In a future study, however, its validity and performance needs to be extensively examined before it can be introduced into clinical practice.

## 7. Conclusion

A novel propofol administration strategy for closed-loop DOH control has been proposed. Evaluation of the proposed control scheme in simulated procedures over wide-ranging PKPD models with parameter perturbations suggested that 1) the closed-loop performance can be significantly enhanced by employing the individualized controller based on the PD model identified using the induction phase response, and that 2) the proposed control scheme is equipped with a sufficient level of robustness against uncertainty in the PK model.

## References

- Åström, K. J. and T. Hägglund (2006): *Advanced PID Control*. ISA.
- Bibian, S. (2006): *Automation in clinical anesthesia*. PhD thesis, Department of Electrical and Computer Engineering, University of British Columbia, Canada.
- Bibian, S., C. R. Ries, M. Huzmezan, and G. Dumont (2005): “Introduction to automated drug delivery in clinical anesthesia.” *European Journal of Control*, **11:6**, pp. 535 – 537.
- Dumont, G. A., A. Martinez, and M. Ansermino (2009): “Robust control of depth of anesthesia.” *International Journal of Adaptive Control and Signal Processing*, **23:5**, pp. 435 – 454.
- Garpinger, O. and T. Hägglund (2008): “A software tool for robust PID design.” In *Proc. 17th IFAC World Congress*. Seoul, Korea.
- Gentilini, A., M. Rossoni-Gerosa, C. W. Frei, R. Wymann, M. Morari, A. M. Zbinden, and T. W. Schnider (2001): “Modeling and closed-loop control of hypnosis by means of bispectral index (BIS) with isoflurane.” *IEEE Transactions on Biomedical Engineering (TBME)*, **48:8**, pp. 874 – 889.
- Haddad, W. M., T. Hayakawa, and J. M. Bailey (2006): “Adaptive control for nonlinear compartmental dynamical systems with applications to clinical pharmacology.” *System & Control Letters*, **55:1**, pp. 62 –70.
- Hägglund, T. and K. J. Åström (2002): “Revisiting the Ziegler-Nichols tuning rules for PI control.” *Asian Journal of Control*, **4:4**, pp. 364–380.
- Ionescu, C. M., R. D. Keyser, B. C. Torricco, T. D. Smet, M. M. R. F. Struys, and J. E. Normey-Rico (2008): “Robust predictive control strategy applied for propofol dosing using bis as a controlled variable during anesthesia.” *IEEE Transactions on Biomedical Engineering*, **55:9**, pp. 2161 –2170.
- Johansen, J. W. and P. S. Sebel (2000): “Development and clinical application of electroencephalographic bispectrum monitoring.” *Anesthesiology*, **93:5**, pp. 1336 – 1344.

- Marsh, B., M. White, N. Morton, and G. N. Kenny (1991): “Pharmacokinetic model driven infusion of propofol in children.” *British Journal of Anaesthesia*, **67:1**, pp. 41 – 8.
- Martinez, A. (2005): “Robust control: PID vs fractional control design, a case study.” Master’s thesis, University of British Columbia, Canada.
- Panagopoulos, H., K. J. Åström, and T. Hägglund (2002): “Design of PID controllers based on constrained optimisation.” *Control Theory & Applications, IEEE Proceedings*, **149:1**, pp. 32–40.
- Schnider, T. W., C. Minto, P. Gambus, C. Andresen, D. Goodale, S. Shafer, and E. Youngs (1998a): “The influence of method of administration and covariates on the pharmacokinetics of propofol in adult volunteers.” *Anesthesiology*, **88:5**, pp. 1170 – 1182.
- Schnider, T. W., C. F. Minto, P. L. Gambus, C. Andresen, D. B. Goodale, S. L. Shafer, and E. J. Youngs (1998b): “The influence of method of administration and covariates on the pharmacokinetics of propofol in adult volunteers.” *Anesthesiology*, **88:5**, pp. 1170 – 1182.
- Schüttler, J. and H. Ihmsen (2000): “Population pharmacokinetics of propofol: A multicenter study.” *Anesthesiology*, **92:3**, pp. 727–738.
- Sheiner, L. B., D. R. Stanski, S. Vozeh, R. D. Miller, and J. Ham (1979): “Simultaneous modeling of pharmacokinetics and pharmacodynamics: Application to d-tubocurarine.” *Clinical Pharmacology and Therapeutics*, **25:3**, pp. 358 – 371.
- Soltesz, K., T. Hägglund, and K. J. Åström (2010): “Transfer function parameter identification by modified relay feedback.” In *Proc. American Control Conference*. Baltimore, USA.
- Struys, M. M. R. F., T. D. Smet, S. Greenwald, A. R. Absalom, S. Bingé, and E. P. Mortier (2004): “Performance evaluation of two published closed-loop control systems using bispectral index monitoring – a simulation study.” *Anesthesiology*, March.
- Viertö-Oja, H., V. Maja, M. Särkelä, P. Talja, N. Tenkanen, H. Tolvanen-Laakso, M. Paloheimo, A. Vakkuri, A. Yli-Hankala, and P. Meriläinen (2004): “Description of the entropy algorithm as

*Paper III. Individualized PID Control of Depth of Anesthesia*

applied in the datex-ohmeda s/5 entropy module.” *Acta Anaesthesiol Scandinavica*, **48:2**, pp. 154 – 161.

Zikov, T., S. Bibian, G. Dumont, M. Huzmezan, and C. Ries (2006): “Quantifying cortical activity during general anesthesia using wavelet analysis.” *IEEE Transactions on Biomedical Engineering*, **53:4**, pp. 617 – 632.